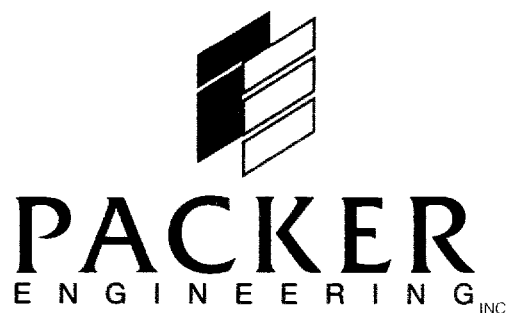


## Appendix G:

### Metallurgical Evaluations of Corroded Pipe Samples

**FERMI LABORATORY  
MAIN INJECTOR COOLING WATER SYSTEM  
CORROSION EVALUATION**

SUBMITTED BY:



**To:**

**Mr. John A. Satti, P.E.  
FERMI NATIONAL ACCELERATOR LABORATORY  
Post Office Box 500  
Batavia, Illinois 60510**

**Fermi Purchase Order No. 505892**

**December 5, 1997**

## **FERMI LABORATORY MAIN INJECTOR COOLING WATER SYSTEM CORROSION EVALUATION**

### **I. INTRODUCTION**

The Main Injector under construction at Fermi National Accelerator Laboratory in Batavia, Illinois contains a cooling water system fabricated from 304L stainless steel. Hydrostatic pressure testing of the piping began in May, 1997, and numerous leaks began to appear at welds in November, 1997, when testing was approximately 66% complete. Packer Engineering was requested to determine the cause of the leakage and assist in developing repair procedures.

### **II. BACKGROUND**

The supply and return cooling water loops are primarily fabricated of 6", schedule 10, 304L SS piping, with 2" drawoffs to cool the magnets. The nominal pipe wall thickness is 0.134" for the 6" and 0.109" for the 2". The sections were tack welded together, and 308 weld material was used to join the piping. Both machine welding and hand welding was utilized. Reportedly for pressure testing, well water which was partially demineralized by portable bottles was used to first test MI-60 to MI-10. As more water was made, this water was pushed forward into MI-10 to MI-20, MI-60 to MI-50 and MI-50 to MI-40. This resulted in hydrostatic test water remaining stagnant in the system for six months.

### **III. OBSERVATIONS**

Packer Engineering was provided with a 23' length of 6" pipe, which contained a water drawoff, and one 20' length with a circumferential weld at each end. Externally, both welds appeared to be of acceptable quality. An external leak was found to be in one of the welds prior to removal of this section. Plates 1 and 2 show the as-received section and the leaking weld. As shown in Plate 3, on the inside of the as-received pipe the welds were stained and contained several corrosion nodules. The portions of the pipe that contained the welds were removed, and the sections were cut lengthwise along the in-service middle axis for visual examination.

Plates 4 through 8 show the condition of the welds after the ID of the pipe was exposed. Both welds contained considerable heat tint from air oxidation during welding. Locations where tack welds were made became hotter, resulting in a wider band of heat tint. It was observed that the corrosion nodules were primarily at locations where tack welds were made, or where there was a lack of fusion. No corrosion nodules were found to be present on the base material away from the welds of the section examined.



Several of the locations that contained nodules were lightly sandblasted to reveal the underlying metallic structure. It appears that the tack welds were not completely consumed by the butt weld leaving a rough surface or a crack. Refer to Plates 9 through 11.

#### **IV. METALLURGICAL EXAMINATION**

Areas that contained the heaviest corrosion nodules were sectioned longitudinally through the center to expose a cross-section of the weld at that point. In each case an internal cavity was exposed that was filled with debris. Energy dispersive spectroscopy (EDS) elemental analysis of the residue recorded the presence of notable concentrations of carbon, oxygen and sulfur. Refer to Plates 12 through 15 for typical photomicrographs, and Figures 1 and 2 for the EDS analyses.

Semi-quantitative EDS analysis of the weld metal indicates that 308 weld rod was utilized, and the microstructure appears representative of acceptable quality material. Refer to Figure 3 for the weld analysis and to Plate 16 for typical microstructures.

#### **V. CONCLUSIONS**

It is our professional opinion that the leaks were caused by microbiologically induced corrosion (MIC), which developed due to the hydrostatic test procedures utilized. This opinion is based on a corrosion morphology quite unique to MIC, and the presence of high concentrations of carbon and sulfur found in the residue in the weld pits. Since high oxide levels along with sulfur is also present in the pits, it suggests that both anaerobic and aerobic bacteria played a role. The corrosion mechanism is a direct result of low pH excretion products released by the bacterial nests which eventually corrodes through the pipe wall.

Over time, stagnant, untreated water will nurture microbiological growths that if undisturbed can form colonies at conducive locations. Such locations usually have irregular or rough surfaces, or are at crevices. Therefore, welds are particularly prone to attack although attack can also begin on smoother areas. MIC has been documented to occur in a variety of alloys, although stainless steel appears to be particularly vulnerable.

In this case, the same warm water remained in the piping system for six months, with only some dilution occurring in that time frame. Based on the pipe section examined, the prime area of microbiological colony development was at tack welds which were not consumed in the butt weld, leaving rough and porous spots. However, a general scale was present on the entire surface of the welds which may also influenced the corrosion. This is due to a lack of adequate shielding on the ID as shown by the vivid oxidation colors adjacent to the welds. No MIC attack was found in the base metal away from the welds.



This report was compiled prior to the completion of the testing and examination of the cooling water system, and conclusions were made after only two welds were examined. In-field radiographic examination of the welds and proper water analysis have yet to be conducted to further verify the conclusions presented herein. Further discussion as to the extent of the problem, along with recommendations on repairs, weld quality and future hydrostatic testing procedures are therefore deferred to a later date.

PACKER ENGINEERING, INC.

Steve Strack  
Manager, Materials Engineering

Kenneth F. Packer, Ph.D., P.E.  
Chief Engineer

/jkw

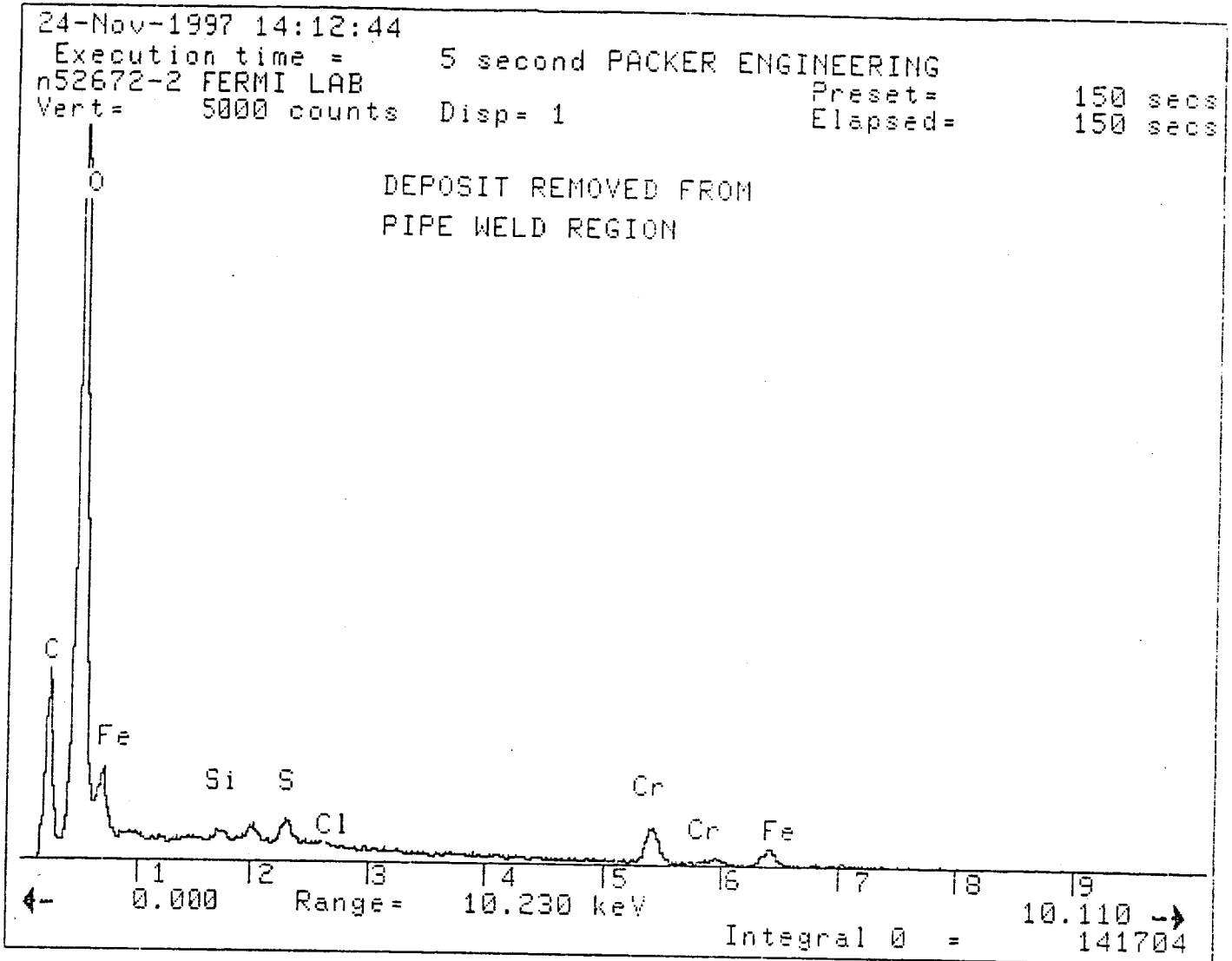


**Figure 1**

Bulk analysis of residue shown in Plate 14. Note the high oxygen and carbon content and the presence of sulfur.



Negative No. 5634E-6

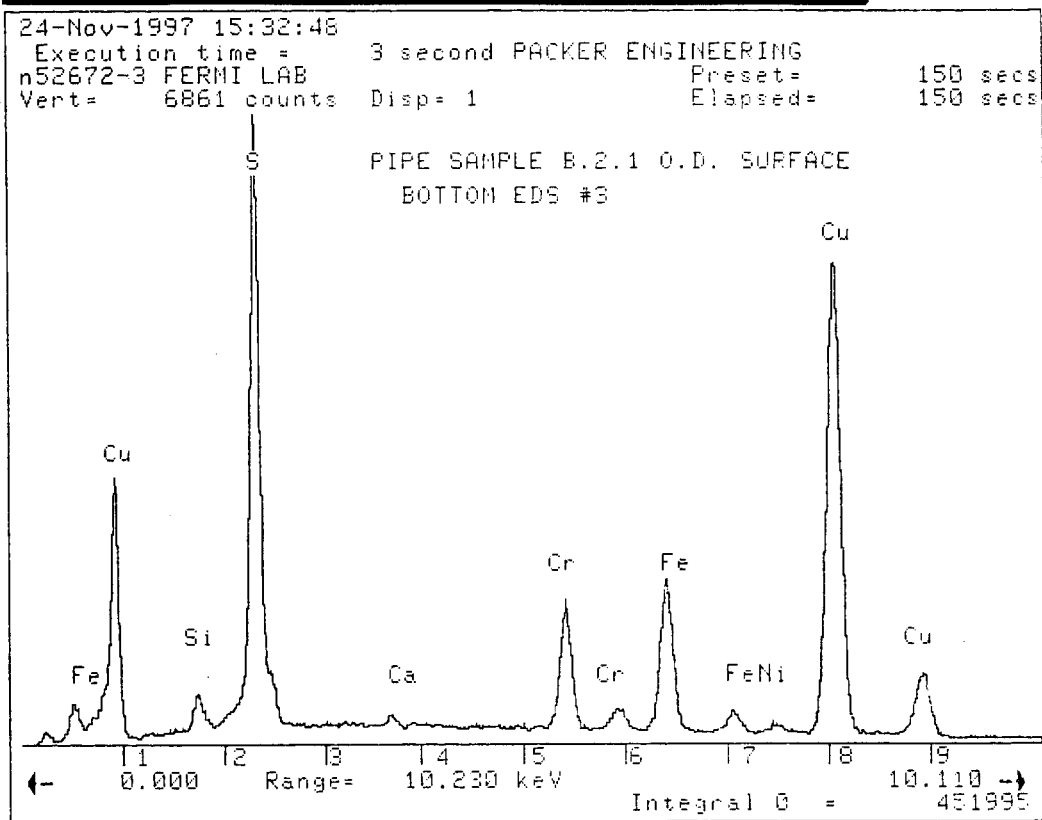
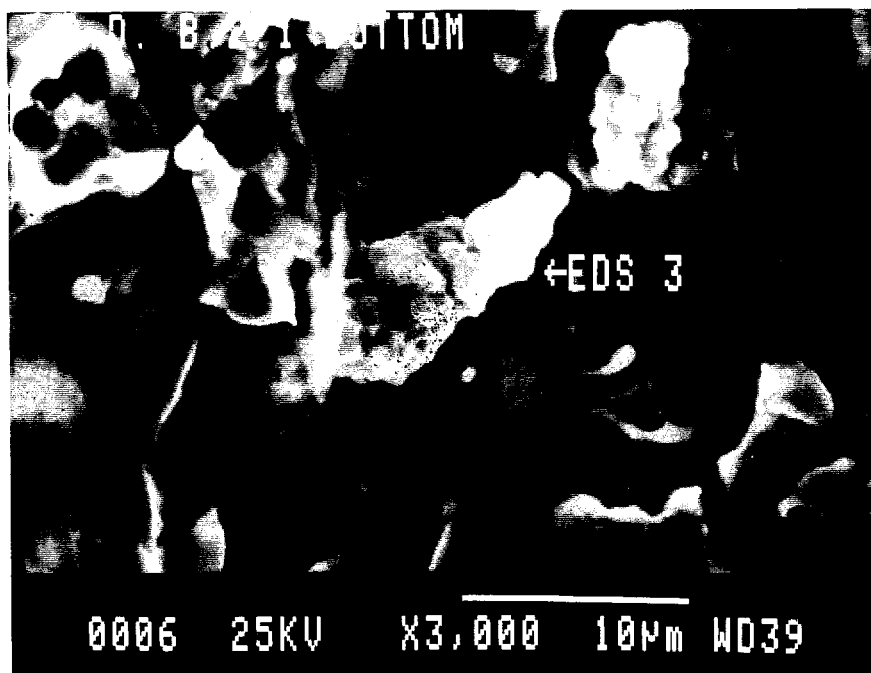


Figure 2

EDS elemental analysis of the growth indicated by the arrow in the photograph. Note the high sulfur content.



26-Nov-1998 08:58:39 N52672-7

Accelerating voltage 20.0 KeV  
 Beam - sample incidence angle 90.0 degrees  
 Xray emergence angle 44.8 degrees  
 Xray - window incidence angle 4.8 degrees

STANDARDLESS EDS ANALYSIS  
 (ZAF CORRECTIONS VIA MAGIC V)

ELEMENT & LINE	WEIGHT PERCENT	ATOMIC PERCENT*	PRECISION 2 SIGMA	K-RATIO**
Cr KA	20.88	22.20	0.08	0.2417
Fe KA	67.81	67.15	0.19	0.6642
Ni KA	11.31	10.65	0.09	0.1041
TOTAL	100.00			

ITERATIONS 5  
 \* NOTE: ATOMIC PERCENT is normalized to 100.  
 \*\* NOTE: K-RATIO = K-RATIO x R  
 where R = reference (standard)/reference (sample)

Normalization factor: 1.000

ZAF Correction Factors

Element	Z factor	A factor	F factor
Cr	0.968	1.049	0.851
Fe	0.972	1.067	0.985
Ni	0.961	1.130	1.000

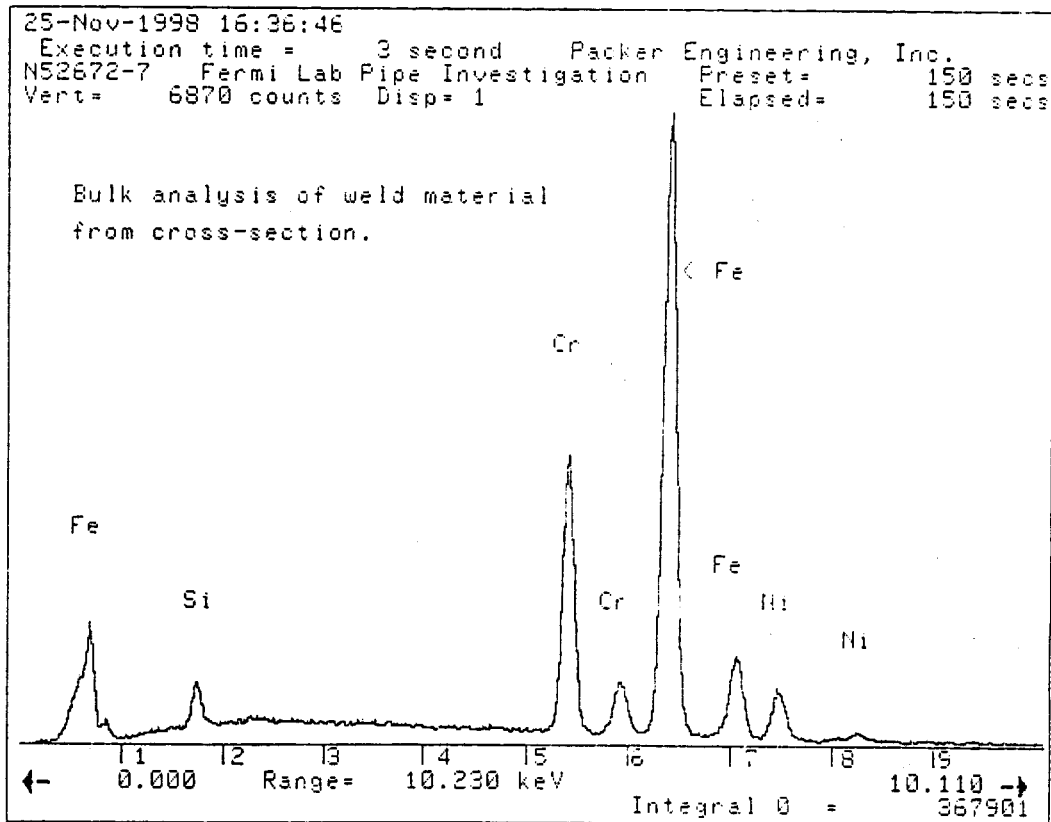
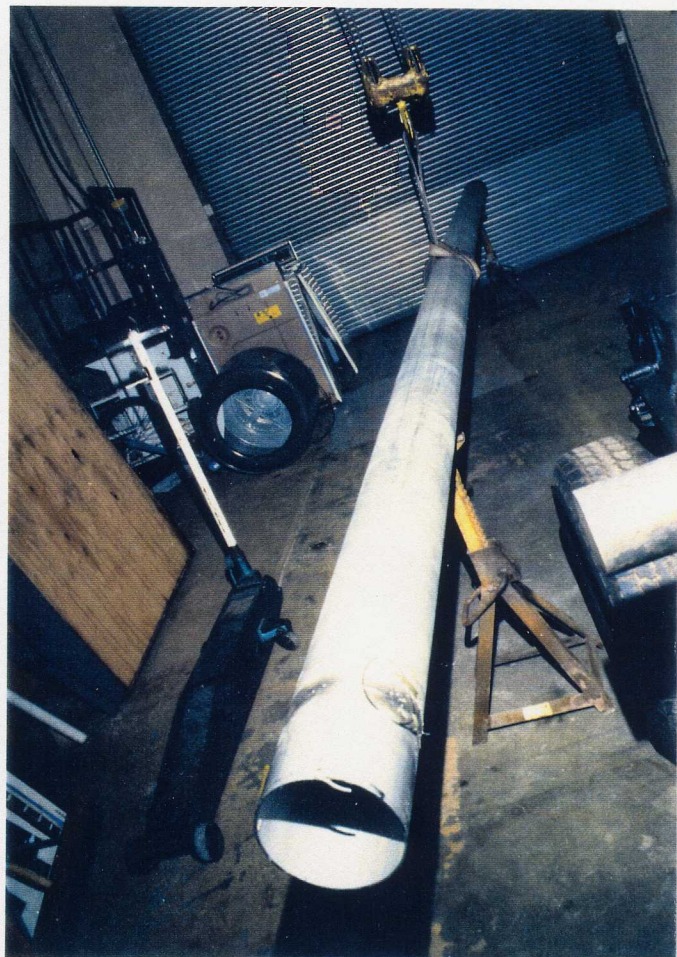


Figure 3  
 Bulk analysis of weld metal.



Negative Nos. 5621E-17 & -7



**Plate 1**  
As-received section of piping.



Negative Nos. 5621E-21 & -29

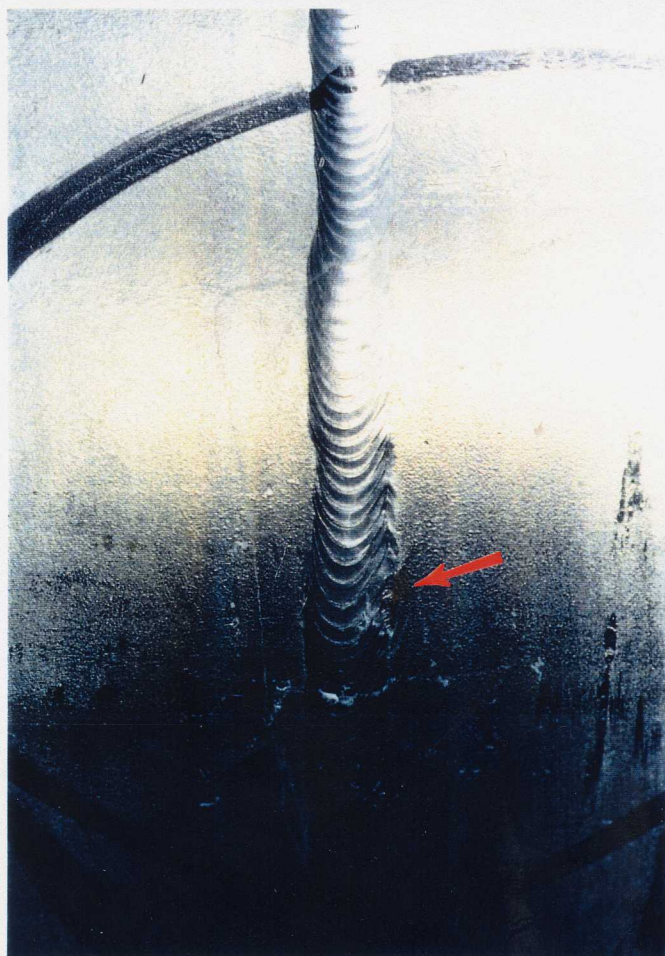
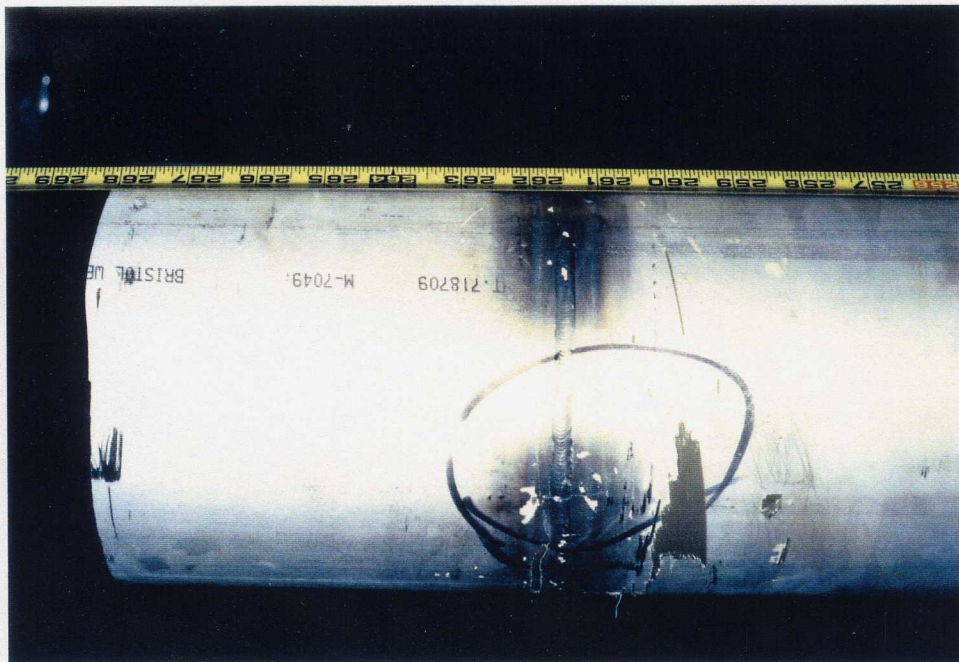
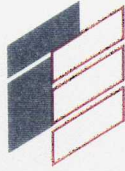


**Plate 2**  
View of a leaking weld  
shown at the arrow.



Negative No. 5621E-13

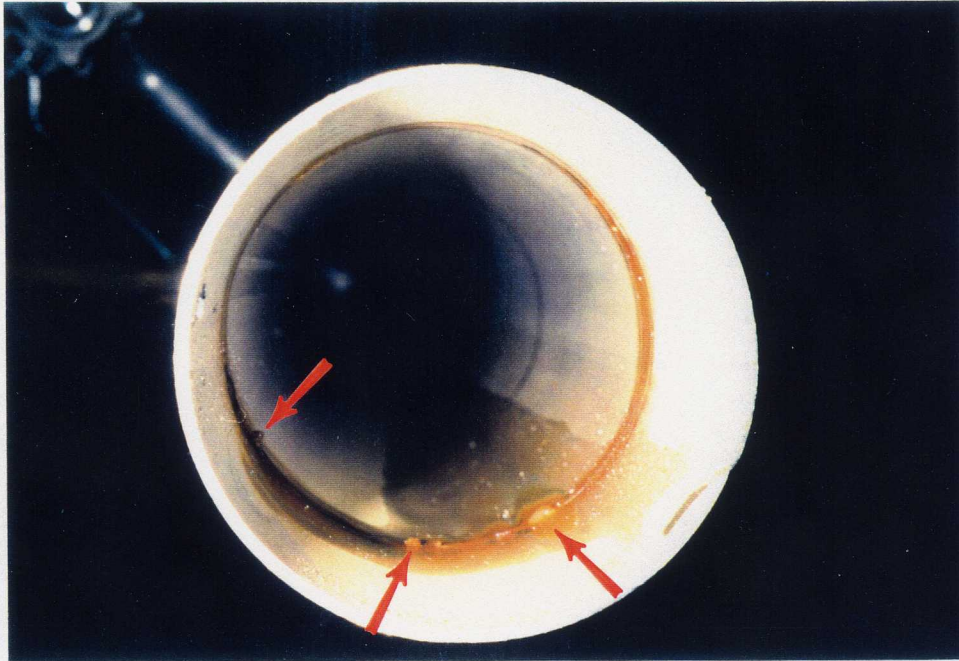


**Plate 3**

View of one weld in the as-received pipe showing corrosion nodules (at arrows).



Negative Nos. 5622E-1 & -24

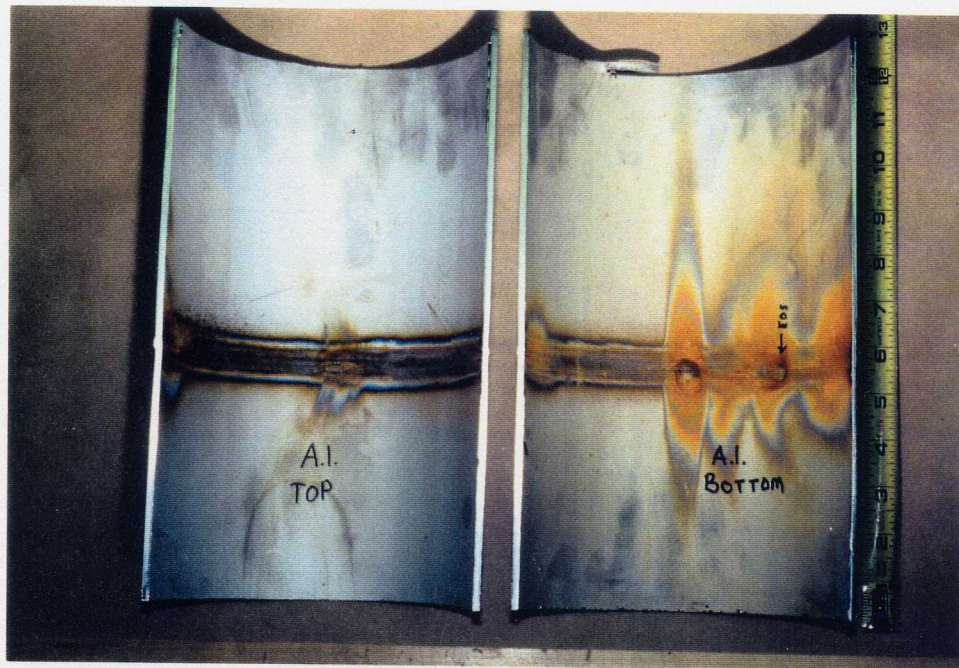


**Plate 4**

Appearance of the two welds in the 6" pipe arbitrarily marked A1 and B2.



Negative Nos. 5622E-5 & -7

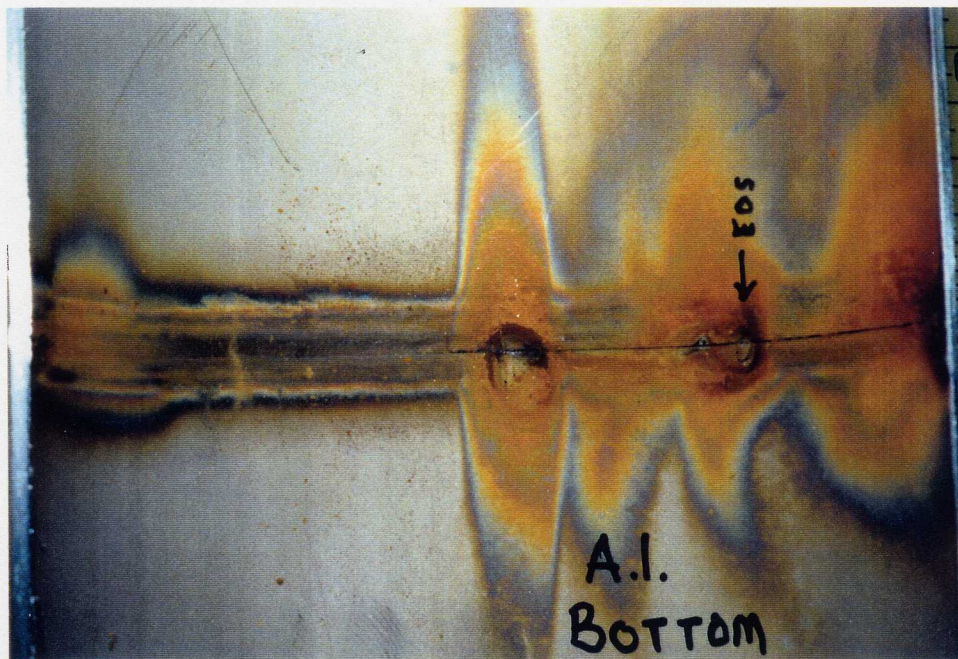
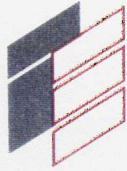


**Plate 5**

Plates 5 through 8 show the appearance of the areas where corrosion nodules are present. Note the lack of fusion on the right hand side of the weld.



Negative Nos. 5622E-11 & -13

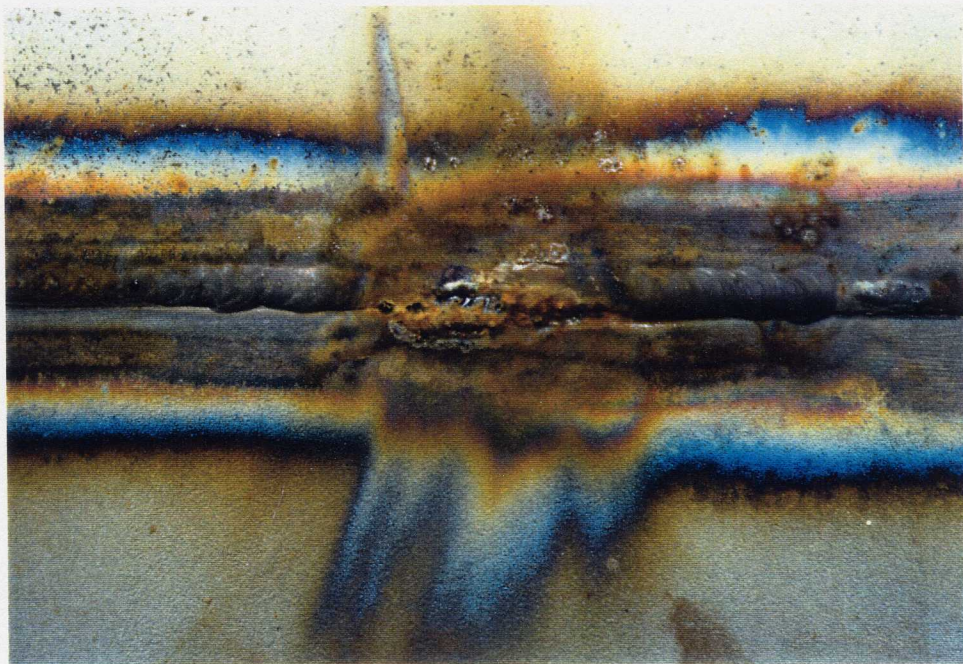
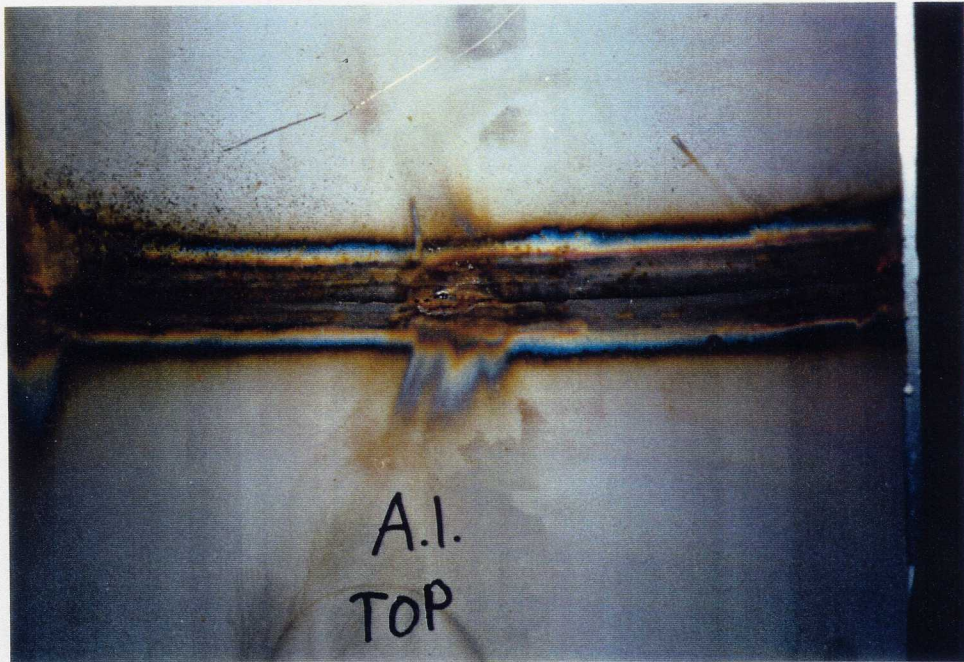


**Plate 6**

The appearance of another area where corrosion nodules are present.



Negative Nos. 5622E-35 & 5637E-3

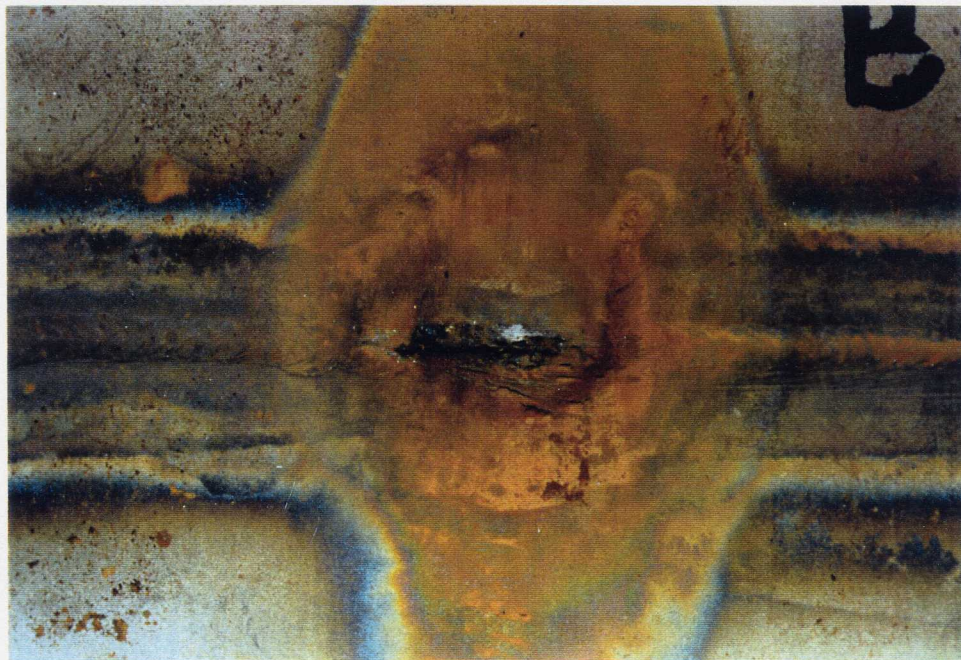


**Plate 7**

The appearance of another area where corrosion nodules are present.



Negative Nos. 5622E-26 & -31

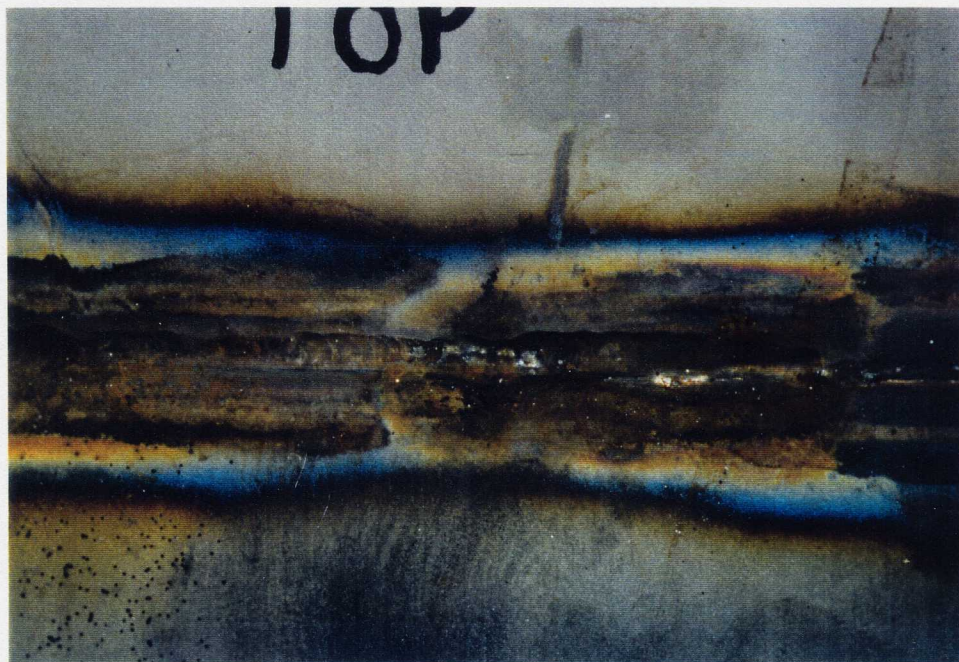


**Plate 8**

The appearance of another area where corrosion nodules are present.



Negative Nos. 5673E-10 & 5675E-16

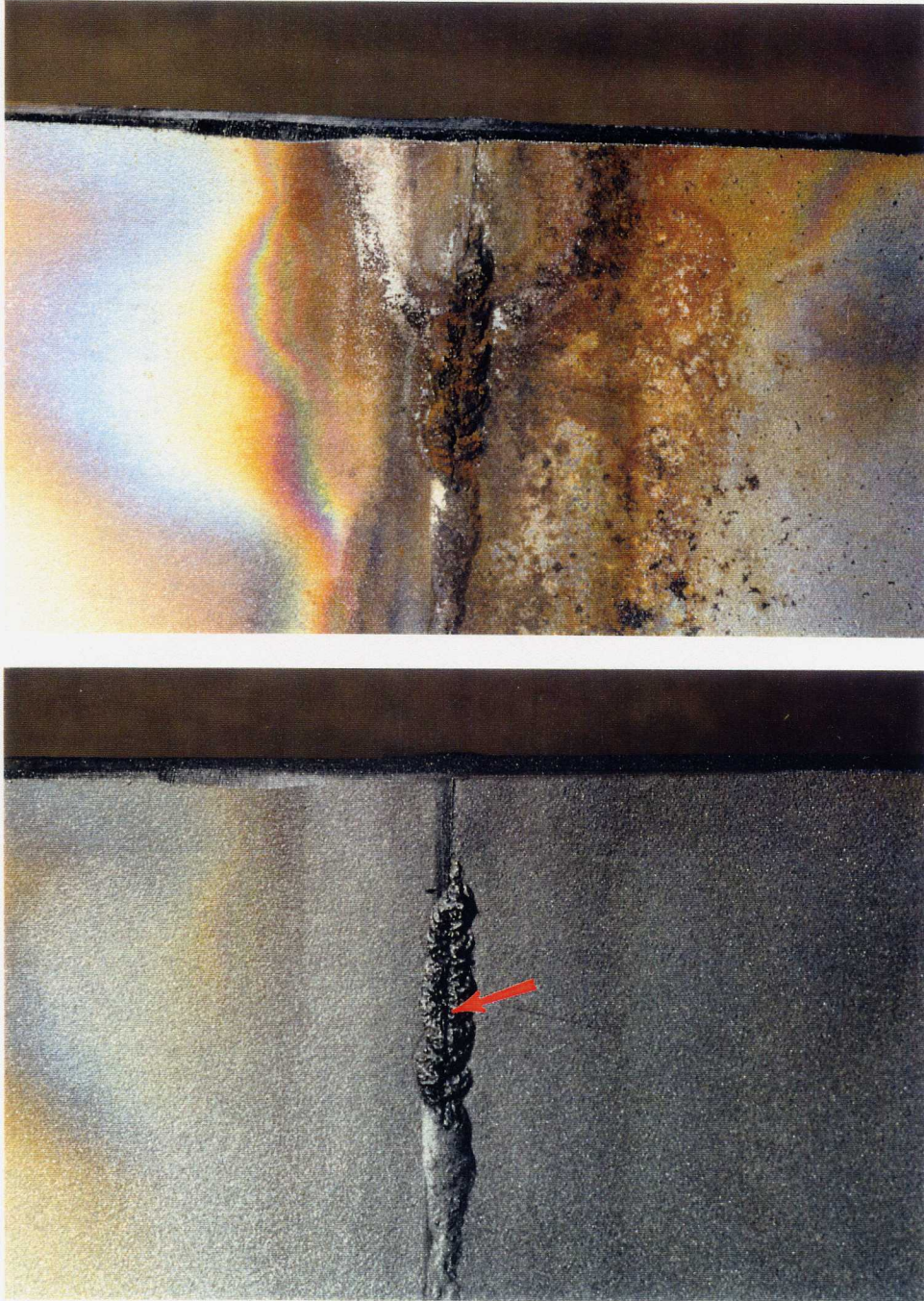


**Plate 9**

Plates 9-11 contain before and after photographs of tack welds that were not consumed and had corrosion nodules on them. Note that during the examination, some of the nodules fell off. Also note crack at arrow.



Negative Nos. 5673E-6 & 5675E-24

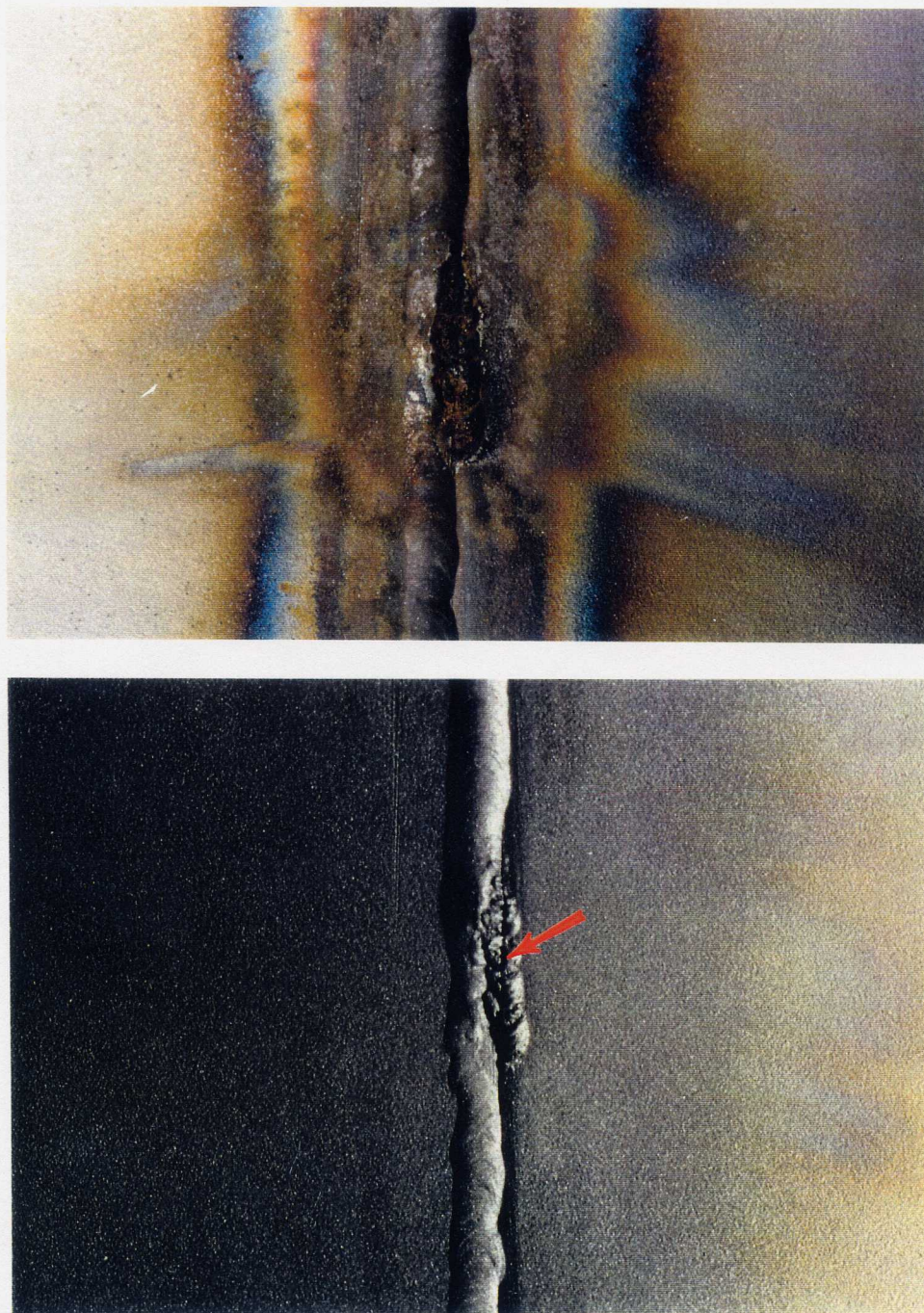


**Plate 10**

Another set of before and after photographs of tack welds that were not consumed and had corrosion nodules on them. Note that during the examination, some of the nodules fell off. Also note crack at arrow.



Negative Nos. 5623E-4 & 5675E-27

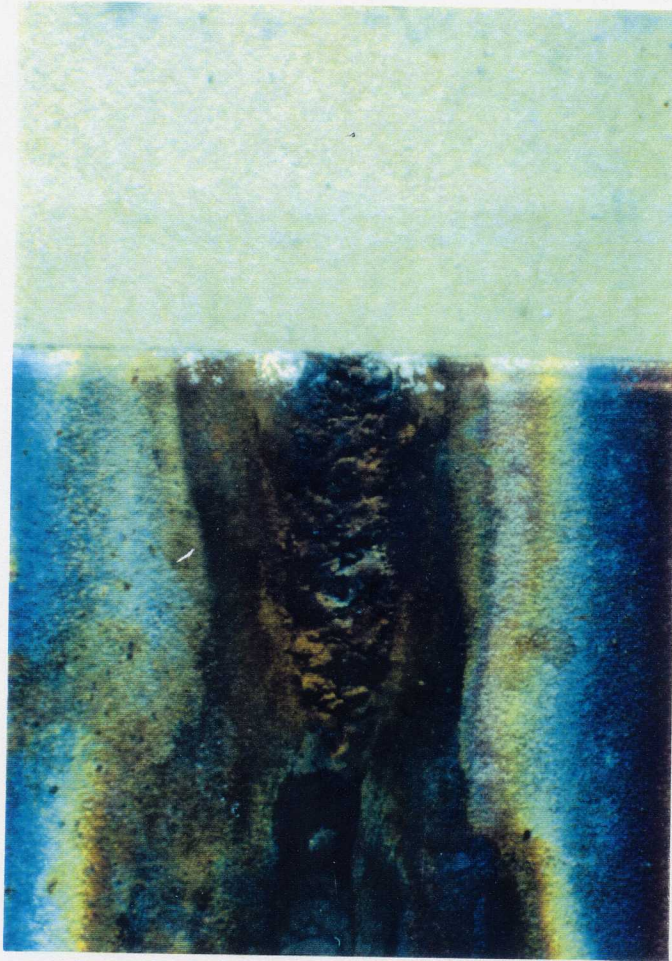
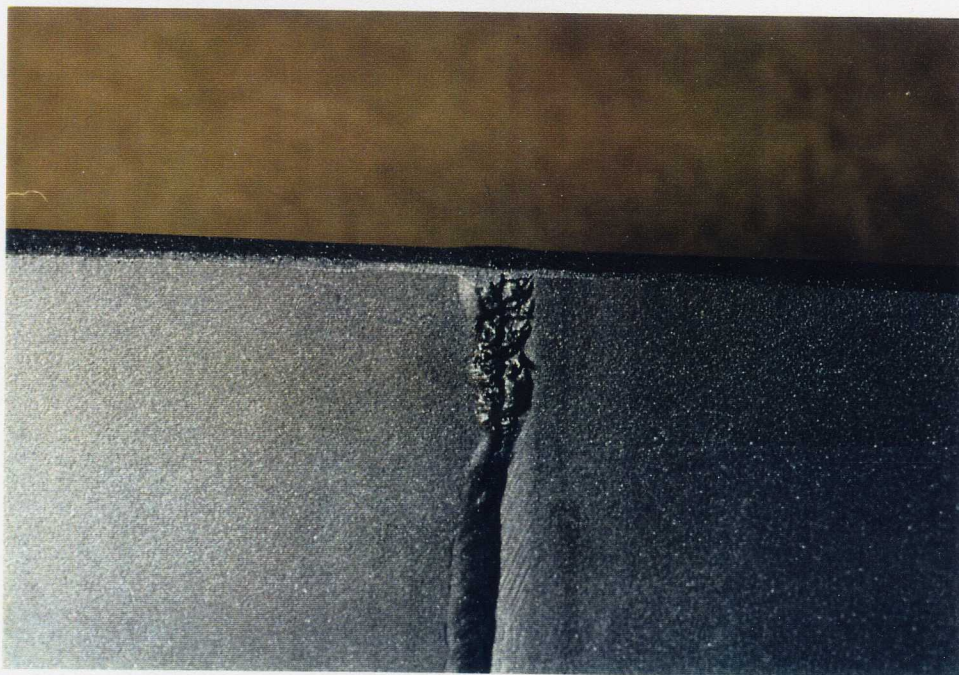


**Plate 11**

Another set of before and after photographs of tack welds that were not consumed and had corrosion nodules on them. Note that during the examination, some of the nodules fell off.





Negative Nos. 5634E-19 & 20

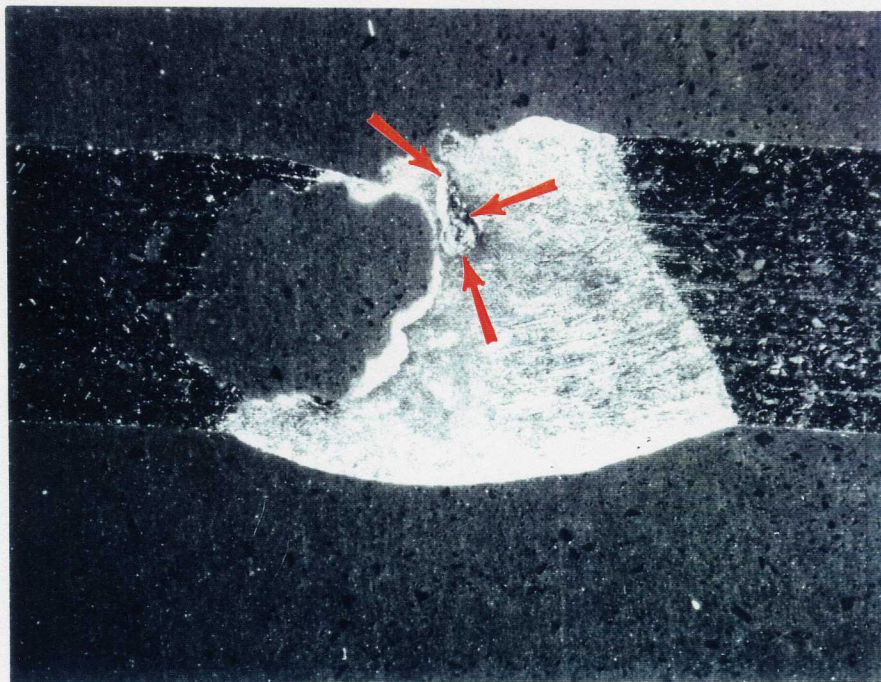
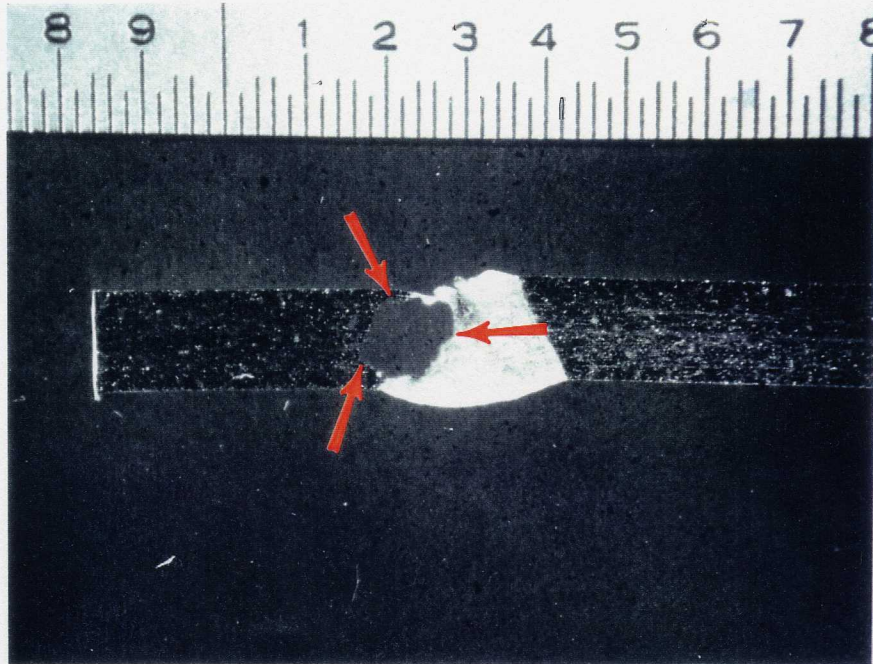


**Plate 12**

Typical cavities found at a module location. (Note that the large cavity filled with the surrounding mounting material when it was mounted for polishing.)

Magnification: 4X (top); 12X (bottom)



Negative No. 5634E-15 & -16

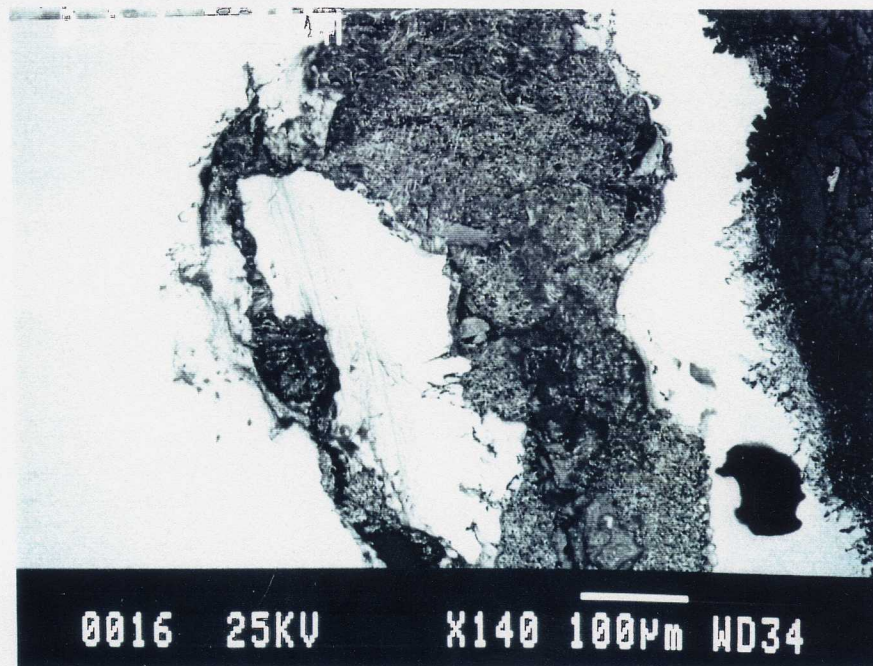
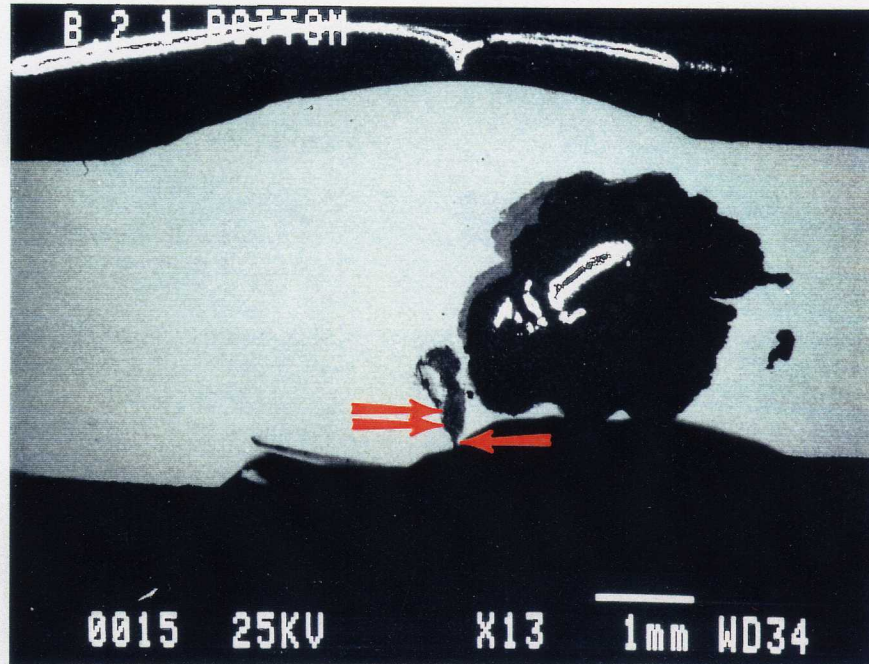


**Plate 13**

SEM photomicrographs of the cavities contained in Plate 12. Note the small tunnel-like entry at the single arrow into the cavity at the double arrows. This tunnel may have originally been a tack weld crack.

Magnification: 13X (top); 140X (bottom)



Negative Nos. 5634E-10 & -11

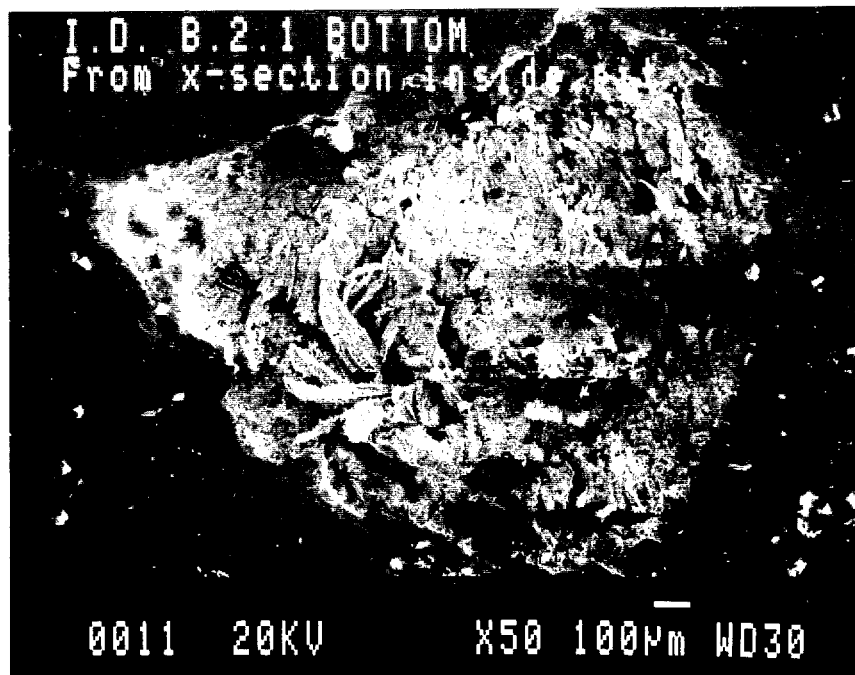
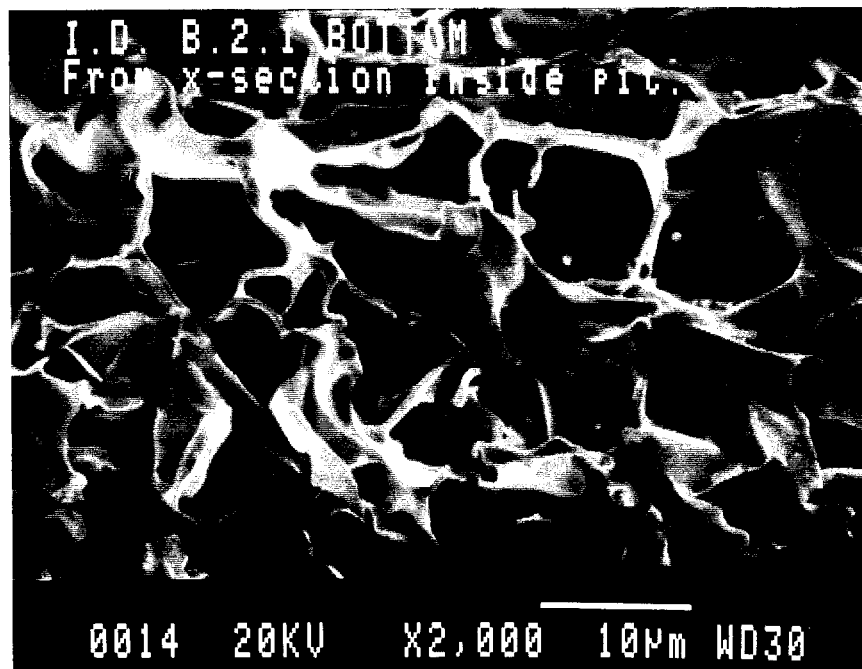
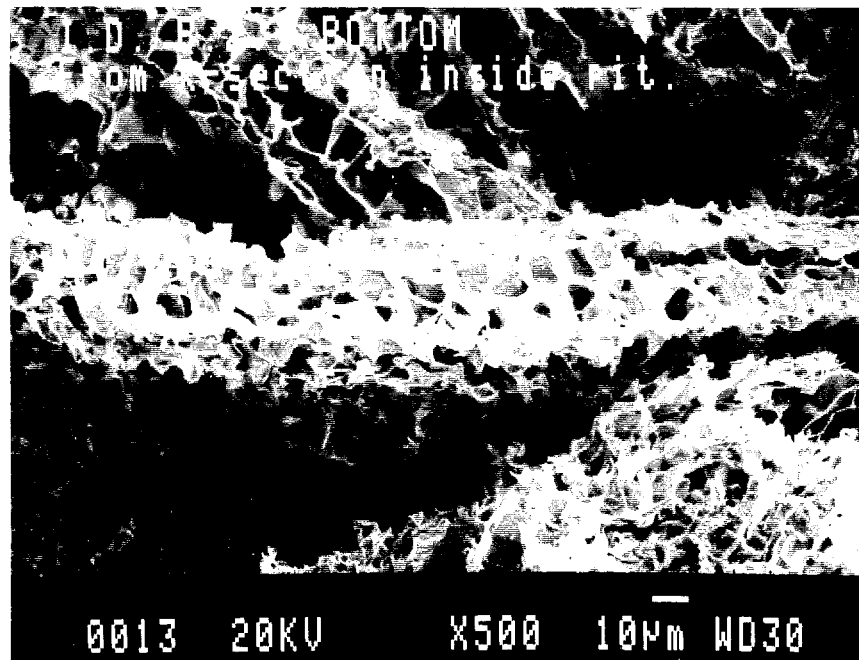


Plate 14

SEM photomicrographs of another cavity still filled with residue.  
Magnification: 17X (top); 50X (bottom)

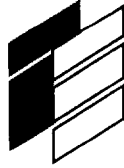


Negative Nos. 5634E-13 & -14



**Plate 15**

SEM photomicrographs of the cavity residue shown in Plate 14.  
Magnification: 500X (top); 2000X (bottom)



Negative Nos. 5690E-1 & -2

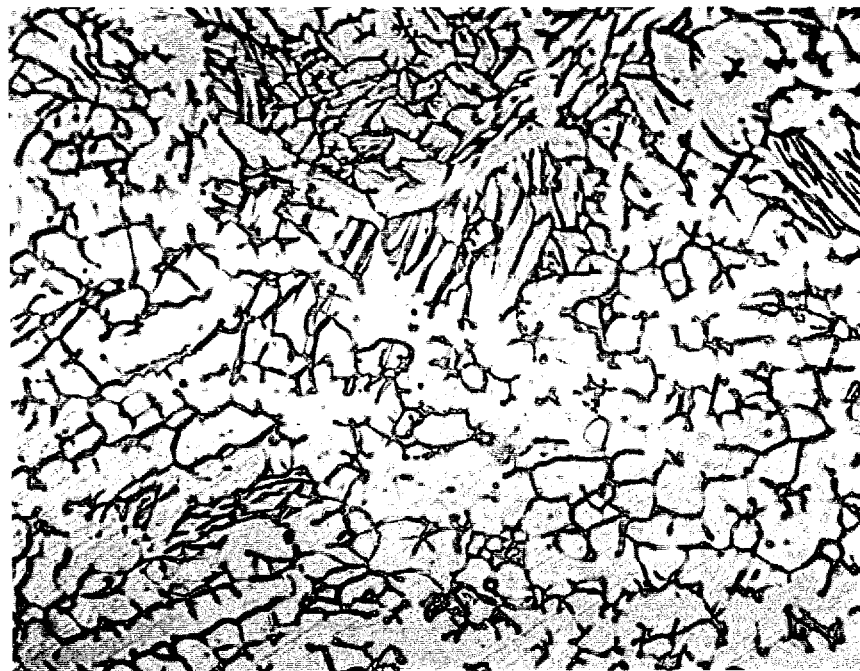
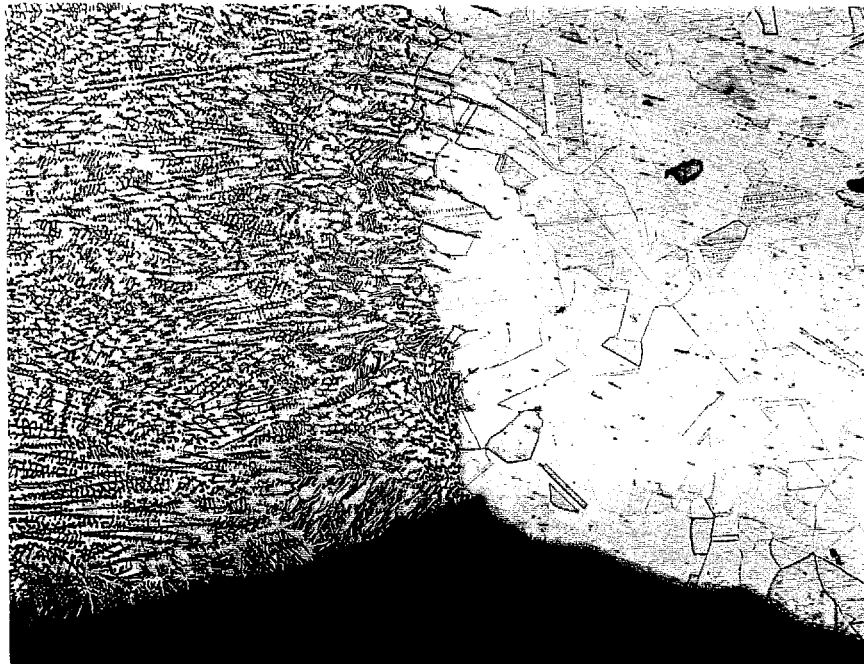


**Plate 16**

Representative microstructure of weld and base material (top) and weld (bottom). The base material consists of equiaxed grains of austenite and the weld consists of ferrite in a matrix of austenite. Both are representative of acceptable quality material.

Magnification: 100X (top); 400X (bottom)

Etchant: 10% Oxalic



# PACKER

ENGINEERING<sup>INC.</sup>

Packer Engineering offers a wide range of services and an international reputation for meeting the needs of our clients ...

**Engineering Disciplines such as:**

- Bioengineering
- Biomechanics
- Chemical
- Electrical
- Engineering Mechanics
- Materials
- Mechanical
- Metallurgical
- Structural/Civil
- Transportation

**Applied to Industries such as:**

- Agriculture
- Chemical Processing
- Extractive Industries
- Manufacturing
- Public Sector/Government
- Service Sector
- Transportation
- Utilities



**FERMI NATIONAL LAB  
BATAVIA, ILLINOIS**

**Nalco Metallographic Analysis No. 092213**

**Specimen:           Injector Ring Q-429**

**Sampling Date:   November 25, 1997**

**CONTENTS**

**A. Nalco Metallographic Analysis Report**

**B. Photographs**

1. As-Received Piping Section with Weld Q-429.
2. Region One Showing a Brown Deposit on the External Surface of the Weld.
3. Region Two Showing Small Deposit Spots.
4. Region Three Showing a Narrow Deposit Strip at the End of an Overlapping Weld.
5. Internal Surface of Piping Section Revealed After Longitudinal Splitting.
6. Region One Showing Misalignment of Pipes at the Circumferential Weld.
7. Region One Showing Corrosion Products.
8. Region Two Showing a Corrosion Nodule.
9. Close-up of Corrosion Nodule in Region Two.
10. Close-up of Corrosion Nodule in Region Two After Cleaning.
11. Region Three Showing Corrosion at Weld.
12. Close-up of Region Three Showing Crevice Present Between Welds.
13. Close-up in Region Three Showing Dendritic Structure of Weld.
14. Coarse Grinding Marks Along Circumferential Weld and Longitudinal Weld Seam.
15. Microstructure in a Transverse Section Through the Pipe.
16. Microstructure in a Longitudinal Section Through the Pipe.

17. Microstructure in a Longitudinal Section Through the Pipe Showing Inclusions.
18. Microstructure of the Longitudinal Seam Weld in Pipe.
19. Microstructure of the Circumferential Weld Joining the Pipes.
20. Close-up of the Microstructure of the Circumferential Weld.
21. External Surface of a Pipe Located Away From the Circumferential Weld.
22. Internal Surface of a Pipe Located Away From the Circumferential Weld.
23. External Surface of the Circumferential Weld in Region One.
24. Close-up of Dendritic Attack Along the External Surface.
25. Internal Surface of Circumferential Weld Showing Misalignment, Incomplete Fusion, and Small Cavities in Region One.
26. Pit Located in Region One.
27. Edge of Pit in Figure 26 Showing Preferential Attack of the Dendritic Phase.
28. Cross Section of the Nodule Located on the Internal Surface in Region Two.
29. Microstructure Present Along the Edge of the Nodule Showing an Interconnected Dendritic Phase.
30. Pit Located in Region Two.
31. Microstructure in the Pit Region Showing Preferential Attack of the Dendritic Phase.
32. Crevice Present Along the Internal Surface in Region Three.
33. Close up of the Tip of the Crevice in Figure 32.
34. Crevice Present Along the Internal Surface.
35. SEM Photo of Surface Lying Dendritic Structure on Internal Surface of Weld Bead.
36. Higher Magnification of Figure 35.
37. SEM Photo of Interdendritic Remnants Present Inside Pit Located in Region One.
38. Higher Magnification of Figure 37.



## NALCO METALLOGRAPHIC ANALYSIS

Analysis No. 092213

FROM: FERMILAB NATIONAL LAB  
BATAVIA, ILLINOIS

## BACKGROUND

A stainless steel cooling water piping system was found to contain numerous leaks after hydrotesting. The piping was intended to supply low conductivity cooling water to magnets of the Main Injector at Fermilab. Reportedly, numerous leaks occurred at the circumferential welds of the system several months after initial hydrotesting of the system. Stagnate water reportedly remained in the system for a period of time after the initial hydrotest. No biocide was added to the stagnate water in the piping.

## DESCRIPTION OF SAMPLE

Received for metallurgical analysis was an 18-1/2" long section of stainless steel piping reportedly removed from the Main Injector cooling system at Fermilab; the pipe has a 6-5/8" outer diameter and an 1/8" wall thickness, Figure 1. The section contains a leaking circumferential butt weld joining two pipes. Mill markings (namely, *WELDED USA A - 312/SA-312 6"*) are present on one of the welded pipe sections. According to Fermilab Specification # 1404 - ES- 333048, the pipe should be 304 stainless steel (Schedule 10) conforming to ASTM-A312 and the circumferential weld should have been done using the inert-gas tungsten-arc (TIG) process with stainless steel filler metal alloy 308. According to the specification documentation a nitrogen purge was to be used to eliminate interior oxidation during welding.

Two welding filler rods and a small coil of wire were included for alloy identification. The two pieces of welding rod were stamped "ER 308L" on one end and had diameters of about 3/32". The welding rod pieces were 15-1/2" long and 20-1/2" long. Similar rods were reportedly used during manual welding. The filler wire was 49" long and had a diameter of approximately 1/32". Similar wire was reportedly used during automatic welding.

Numerous markings were written in black marker on the external surfaces of the as-received section to indicate orientation and position of the piping in service. The circumferential weld is identified with the marking Q-429. The locations of apparently adjacent (not present on the received section) welds 430 and 428 are also indicated on the section, Figure 1. The words Aisle, Floor, Wall, and Top are marked on one end of the section. A reference mark is present near the weld. The reference mark, a



## NALCO METALLOGRAPHIC ANALYSIS

Analysis No. 092213

FROM: FERMI NATIONAL LAB  
BATAVIA, ILLINOIS

line attached to a circle and arrow, is located between the Aisle and Floor markings. This reference mark reportedly corresponds to a point used to identify the areas where x-ray radiographs were made on the weld. The position of weld features discussed in this analysis are given with respect to this reference mark. Measurements are given from the reference mark in the direction of the arrow along the external circumference.

The external surface of the section is essentially free of deposits and oxides, and the surface is mostly smooth. The metal has been ground or abraded along a 1-3/4" wide band centered on the weld bead.

Close examination of the external surface of the weld revealed three sites where perforations in the pipe may have existed. Each site was numbered "1, 2 or 3" using a red grease pen. Two of these sites were subsequently proven to contain large cavities. A 3/8" diameter brown deposit centered along the toe of the weld was designated as region one, Figure 2. Region one is located approximately 4-5/16" from the reference mark and occurs near the orientation labeled "FLOOR" on the pipe. Region two is an area where small brown and green deposits were observed, Figure 3. Region two is located approximately 15-11/16" from the reference mark and along the orientation labeled "TOP". A 1-3/8" long weld overlaps the initial circumferential weld, Figure 4. The overlapping weld has a concave crown for most of its length, which starts 19-1/2" from the reference mark. A narrow, brown deposit strip is present at the end of the overlapping weld, and the surrounding area is designated region three.

The section was longitudinally split to reveal internal surfaces, Figure 5. The markings written on the internal surface correspond to the markings on the external surface. A heat tint band, approximately one inch wide, straddles the weld. The band widens on one side in region three at the site of the overlapping weld.

The internal surface away from the weld is mostly free of significant deposits and oxides; along the circumferential weld, heat tint is present. Brown deposits and oxide patches are present where possible perforations were identified. A large area surrounding region one is covered by orange corrosion products, Figures 6 and 7. The misalignment of the pipes in this region was as much as 0.039", as measured by a calibrated point micrometer.



## NALCO METALLOGRAPHIC ANALYSIS

Analysis No. 092213

FROM: FERMI NATIONAL LAB  
BATAVIA, ILLINOIS

A corroded nodule is present on the internal surface of region two, Figures 8 and 9. Small specks of material are present on the side of the weld adjacent to weld 428, Figure 8. The corrosion products on the nodule are porous and easily removed by scraping with a sharp pick. The underlying material of the nodule is very hard. The surface beneath the nodule contains many fissures, Figure 10. The pipes are misaligned as much as 0.050" in this region.

A thin layer of brown corrosion products overlies an area near the circumferential weld in region three, Figure 11. Specks of material, similar to those observed in region two, were confined to one side of the weld. These specks of material are largely isolated to areas where corrosion has occurred. A circumferentially oriented fissure, approximately 1/2" long, runs along the weld centerline, Figure 12. The fissure is present beneath the overlapping weld observed on the external surface. When examined under a low power stereomicroscope fan-shaped striations strongly resembling dendrites paralleling the internal surface are visible on the weld bead, Figure 13. The striations are observable at most locations along the internal surface weld not obscured by corrosion products. The misalignment of the pipes in region three was as much as 0.055".

Corrosion products were observed at one other region along the internal surface of the weld. The region is located approximately 10-1/2" from the reference point, and the corrosion products are not as heavy as in the other regions.

Longitudinal weld seams are present. The longitudinally oriented weld seams were produced during fabrication of the piping. The longitudinal weld seams show no significant corrosion or corrosion products, Figure 14.

Grinding marks are present at scattered locations along the circumferential weld, Figure 14. Grinding may have been used to clean off possible contaminants prior to welding. No corrosion was observed at the grinding marks.

## ALLOY IDENTIFICATION

Pieces from both pipes, the weld bead, the welding filler rod and wire were submitted to an independent testing laboratory for alloy identification. Results of these analyses are shown in Table 1.

**NALCO METALLOGRAPHIC ANALYSIS**

Analysis No. 092213

**FROM: FERMI NATIONAL LAB  
BATAVIA, ILLINOIS**

Carbon and nitrogen were measured according to test method ASTM E1019-93; other elements by ASTM E1085-87. The compositions measured in both pipe sections correspond to type 304L stainless steel. The welding rod and wire have increased amounts of chromium and nickel compared to the pipe wall away from welds. The composition of the automatic welding filler wire corresponds to a type 308L stainless steel. However, the nickel concentration of the manual welding filler rod (9.93%) was very slightly below the value specified for type 308L stainless steel (10.0-12.0%). The weld bead has chromium and nickel concentrations that are between the pipe and filler metal values, which may be expected from dilution of the filler metal by pipe metal. Note that the nitrogen concentration of the weld bead did not noticeably increase from the values present in the pipe and filler metal.

Magnetic measurements were made to determine ferrite content in the circumferential weld bead using an Elcometer/Inspector Ferrite Indicator Scale 6F. The ferrite content ranged from 5-1/2 to 6%, measured at five locations along the weld. These measurements give an overall ferrite content of the weld, and do not account for microscopic variations that may exist within the weld. The ferrite contents are somewhat higher than acceptable values to prevent hot cracking, typically 3 to 4% in the as deposited weld.

**MICROSCOPIC EXAMINATIONS**

Seventeen specimens were cut from the piping, mounted in a phenolic resin, polished and were etched using standard metallurgical techniques. The mounted pieces were examined with an optical microscope at magnifications up to 1000 diameters. Both transverse and longitudinal sections through the pipe show microstructures composed predominantly of twinned austenite grains, Figures 15 and 16. An unetched longitudinal section shows that some non-metallic inclusions are strung out in the direction of the longitudinal pipe axis, Figure 17.

The longitudinal seam made during manufacture of the pipe was formed by an internal and an external weld, Figure 18. The internal and external surfaces of the seam welds are smooth and show no evidence of corrosive attack. The microstructure of the fusion zone in the seam welds is dendritic.



## NALCO METALLOGRAPHIC ANALYSIS

Analysis No. 092213

FROM: FERMI NATIONAL LAB  
BATAVIA, ILLINOIS

The fusion zone of the circumferential weld has a dendritic microstructure, Figures 19 and 20. No gross evidence of carbide formation was observed in the weld heat affected zone.

The pipe external surface away from the circumferential weld is largely free of deposits or oxides and has a mostly smooth contour, Figure 21. The internal surface of the pipe away from the weld is also mostly smooth and contains little deposits and oxides, Figure 22.

The external surface of the crown on the circumferential weld in region one has scattered areas containing small hemispherical pits that undercut the surface in places, Figure 23. In addition, this surface has areas of shallow preferential attack of the dendritic phase, Figure 24.

A cross section through the weld in region one shows misalignment of the pipes at the weld, incomplete fusion, and cavities contained in the fusion zone at the internal surface, Figure 25. A large pit is present in this region that penetrates into the fusion zone of the weld at least 0.1", Figure 26. The edges of the pit are mostly curved and show evidence of preferential attack of the dendritic phase, leaving behind the skeletal remnants of the interdendritic phase, Figure 27.

The nodule on the internal surface in region two is dendritic, Figures 28 and 29. No cavities are observed in this cross section. The surface profile shows that the nodule has some smooth, wide fissures scattered along its contour. A longitudinal section near the nodule shows a very large pit that extends nearly 90% through the thickness of the weld from the internal surface, Figure 30. The pit is filled with remnants of the interdendritic phase, Figure 31.

A narrow fissure penetrates about 30% of the weld thickness from the internal surface in region three, Figure 32. The tip of the fissure turns back towards the surface, Figure 33. No evidence of deformation is observed along the edges of the fissure. Microstructural features appear discontinuous across the fissure. No microstructural discontinuities are observed in the area immediately below the tip of the fissure. A small fissure, penetrating the weld fusion zone from the internal surface about

**NALCO METALLOGRAPHIC ANALYSIS**

Analysis No. 092213

**FROM: FERMIL NATIONAL LAB  
BATAVIA, ILLINOIS**

0.02", is present at the other region where corrosion was observed, Figure 34.

**SCANNING ELECTRON MICROSCOPY**

An energy dispersive spectrometer system on a scanning electron microscope was used to analyze alloy compositions of the metal, corrosion products, and inclusions; results are listed in Table 2.

Alloy compositions taken from large sampling areas in the microstructure indicate that the weld bead has higher concentrations of chromium and nickel than the metal in the pipe. There are negligible differences in composition between measurements made at the edge and center of the weld bead. Non-metallic inclusions in the pipe microstructure contain increased concentrations of manganese over the bulk composition; in addition, titanium and aluminum are also present.

Corrosion products on the internal pipe surface typically show increased amounts of chromium and manganese and decreased amounts of nickel. High concentrations of chlorine, sulfur, and calcium were also observed at some sites. Small amounts of calcium and sulfur were observed in the irregular deposits to the sides of the weld located where corrosion was observed on the internal surface.

Long, continuous dendrites parallel the internal surface and stand out in relief, Figures 35 and 36. The coarse dendrites have lower chromium and nickel concentrations than the smooth, adjacent interdendritic phase. The interior of the pit found in region one shows skeletal remnants of the interdendritic phase, Figures 37 and 38. The interdendritic phase has much higher concentrations of chromium than the base metal composition. Higher chromium concentrations are also observed at areas surrounding the preferential wastage on pit edges.

**CONCLUSIONS**

The received circumferential weld on the piping section contains a few fissures and large cavities in the fusion zone of the weld. The cavities were formed by preferential attack of the weld dendritic phase and resulted in wall perforations. Microorganisms likely accelerated attack. The fissures appear to be defects from the welding process. Additionally, weld defects such as lack of



## NALCO METALLOGRAPHIC ANALYSIS

Analysis No. 092213

FROM: FERMI NATIONAL LAB  
BATAVIA, ILLINOIS

fusion and weld imperfections such as high ferrite content and also high heat input are present.

Corrosive attack of the dendritic phase occurred by a microstructural galvanic mechanism. The compositional differences between the dendritic and interdendritic phases produce the driving force for corrosion. The dendritic phase has lower chromium content which makes the dendrites less noble than the interdendritic phase. The dendritic phase corrodes when a galvanic circuit is completed by submersion in water. A skeletal network of the more noble interdendritic phase remains after attack.

Critical factors concerning galvanic corrosion are the galvanic potential between the phases, the conductivity of the fluid, and the "area effect". The high heat input of the weld results in increasing the tendency for galvanic corrosion by increasing compositional partitioning (and hence galvanic potential difference) during slow solidification. In addition, slow solidification increased the amount of large, interconnected, surface lying dendrites which may also accelerate attack.

High chromium concentrations in stainless steels typically result in thin, protective oxide layers on the alloy surface. This oxide may be sufficient to limit the current flow required for the galvanic circuit to operate efficiently. Thus, the presence of a non-protective oxide layer or depassivation of a protective oxide layer on surface is required to allow the galvanic circuit to become operative. It is possible that the hint tint formed during welding resulted in an oxide layer that was porous and non-protective, and thus, accelerated attack.

Analytical laboratory reports from Nalco on water samples taken from the cooling water system on November 21, 1997 (included with this report) indicate that anaerobic sulfate reducing bacteria were present in levels of 29 colony forming units per ml. Attack by sulfate reducing bacteria may result in depassivation of the protective oxide layer of the stainless steel, thus exposing the underlying phases to water to complete the galvanic circuit.

It is important to note that the presence of sulfate reducing bacteria in the water samples alone is not direct proof that microbiologically influenced corrosion was active in this system. Complete diagnosis requires that the biological organisms, the



## NALCO METALLOGRAPHIC ANALYSIS

Analysis No. 092213

FROM: FERMI NATIONAL LAB  
BATAVIA, ILLINOIS

morphology of attack, the corrosion products and deposits, and the environment must all be consistent with microbiologically influenced corrosion.

Sulfate reducers can cause intense localized attack in the form of hemispherical depressions, and the interiors of resulting pits are characteristically smooth. However, the cavities in the present case typically have rough edges due to selective attack. In addition, shallow attack was observed on the external surface of the pipe at its lowest point where leaking water may collect (labeled with the floor orientation). Anaerobic bacteria can not be the direct cause of external attack. However, leaking pit contents may be highly acidic if acid-producing bacteria were within cavities, and hence, may explain the external surface wastage.

Some evidence points to contributory corrosion mechanisms other than microbiologically influenced corrosion. For example, the longitudinal seam weld was not attacked, nor were internal surfaces away from the circumferential weld. Thus, it is clear that the corrosion resistance of the installation welds is lower than the intact pipe wall or the seam welds. However, microbiologically influenced corrosion probably acted as a major contributing corrosion mechanism by depassivating the less corrosion resistant welds.

The combination of the weld microstructure and the aggressiveness of the environment resulted in the failure. It is possible that removing one of these factors may have prevented or at least reduced the risk of failure.

Thus, remedies for corrective action must address these factors. First, defects such as misalignment of the pipe and fissures should be prevented during the welding process. Such defects provide sites for concentration of corrosive species in the water. Imperfections in the weld such as excessive heat tint may be minimized by properly using a nitrogen blanket during welding, chemically cleaning the surfaces after welding (highly recommended), and reducing the heat input during welding. Reducing the heat input should also be beneficial in reducing segregation and excessive formation of ferrite in the microstructure of the fusion zone of the weld. Note that the longitudinal seam of the pipe, which utilizes a multipass welding operation with lower heat



## NALCO METALLOGRAPHIC ANALYSIS

Analysis No. 092213

FROM: FERMI NATIONAL LAB  
BATAVIA, ILLINOIS

input and no filler metal, did not show any evidence of corrosive attack. Thus, improved welding techniques may have reduced or possibly prevented attack.

One other filler metal, type 347 stainless steel, is acceptable by code as a welding rod for joining type 304L stainless steel piping. Type 347 has lower chromium concentration (17.0-19.0), a wider nickel range (9.0-13.0), and a higher allowable carbon limit (0.08) than type 308L stainless steel. In addition, small additions of niobium and/or tantalum are added that combine with carbon, thus preventing the formation of chromium rich carbides (and hence, sensitization) during welding. Use of type 347 stainless steel welding rods may possibly decrease the ferrite content of the as-deposited weld. However, the lower chromium content may also result in higher corrosion rates offsetting other beneficial effects. Fully austenitic welds may be produced using other welding rods, thus largely eliminating or reducing microstructural galvanic effects. However, severe hot cracking may occur unless extremely low concentrations of impurities are present. Additionally, even if done well, fully austenitic welds would likely be much more crack sensitive than duplex welds.

Use of chemical treatments such as biocides should effectively reduce the colonies of microorganisms that may have contributed to the problem. However, after repairing defective welds, it is strongly recommended that the internal surfaces be cleaned using a caustic rinse, followed by a dilute nitric acid wash.

P.B. DESCH / H.M. HERRO

PBD / HMH  
1/28/98

**TABLE 1. ALLOY IDENTIFICATIONS**

(Values are given in atomic percent)

	Pipe (Q430- Q429)	Pipe (Q429- Q428)	Weld Wire Automatic	Weld Rod Manual	Weld Q429	304L*	308L*
Fe	bal.	bal.	bal.	bal.	bal.	bal.	bal.
Cr	18.64	18.42	19.89	20.17	18.81	18.0- 20.0	19.0- 21.0
Ni	8.14	8.33	10.24	9.93	8.57	8.0-12.0	10.0- 12.0
Mn	1.71	1.71	2.07	1.68	1.62	<2.00	<2.00
Si	0.63	0.32	0.78	0.39	0.63	<1.00	<1.00
Cu	0.34	0.35	0.05	0.16	0.32		
Mo	0.37	0.43	0.13	0.12	0.38		
C	0.02	0.02	<0.01	<0.01	<0.01	<0.030	<0.030
N	0.095	0.088	0.081	0.100	0.092		
P	0.029	0.028	0.021	0.020	0.028	<0.045	<0.045
S	0.020	0.021	0.012	0.008	0.022	<0.030	<0.030

\* Compositions for 304L and 308L alloy designations are taken from the Metals Handbook Ninth Edition, Volume 3 - Properties and Selection: Stainless Steels, Tool Materials and Special-Purpose Metals, American Society for Metals, Metals Park, OH, (1980).

**TABLE 2 RESULTS FROM ENERGY DISPERSIVE X-RAY ANALYSIS**

(All values are in elemental weight percent neglecting oxygen)

Element	Fe	Cr	Ni	Ti	Mn	Cu	Mo	Al	Si	P	S	Cl	Ca
<b>Overall Alloy Compositions</b>													
Pipe	70.91	18.01	8.31		2.21				0.55				
Weld - Edge	70.02	18.59	8.75		2.14				0.50				
Weld - Center	69.79	18.40	8.74		2.52				0.54				
<b>Inclusions</b>													
	35.10	36.77	3.25	2.20	19.76			2.71	0.19				
	53.62	28.00	5.80	0.37	10.95			1.14	0.11				
<b>Corrosion Products on Internal Surfaces</b>													
	39.02	39.54	5.35		2.30	0.84			0.47		1.05	11.43	
	24.70	55.21	2.99		3.77	1.23			0.47		5.31	6.32	
	64.85	21.85	5.98		3.47	1.41			1.50		0.36		0.56
	50.74	35.22	2.63		7.61	0.92			1.93		0.45		0.50
	45.37	44.51	1.61		2.20	1.23	2.31		1.29				1.40
	44.47	42.60	1.28		4.81	4.27	0.35		0.80				0.68
<b>Bumpy Deposits on Internal Surface on the Pipe</b>													
	59.05	29.62	3.80		4.06	1.14			1.22		0.70		0.33
	73.77	18.03	3.29		2.62	0.65			1.49		0.50		0.29
	74.44	15.97	4.98		2.66	0.40			0.80				0.15
	62.00	25.71	3.70		3.58	1.47			2.05				0.78
<b>Interdendritic Material Remaining in Pit</b>													
	62.81	28.18	2.74		2.40	0.92	0.75		1.73				
	62.71	28.71	2.94		2.68	0.73	0.69		1.34				
<b>Dendritic Phase on Surface of Welds</b>													
	75.61	13.36	4.46		1.66	1.26	0.94		2.26	0.11			0.34
	76.45	10.55	3.55		1.34	1.65	0.64		3.80	0.88			
<b>Interdendritic Phase on Surface of Welds</b>													
	72.04	16.47	6.75		2.37	0.76			1.26		0.34		
	72.66	16.66	6.31		1.80	0.83			1.40		0.33		
<b>Material Surrounding Attacked Phase</b>													
	68.65	23.53	4.7		1.68				1		0.44		
	70.86	19.02	7.17		2.16				0.46		0.33		

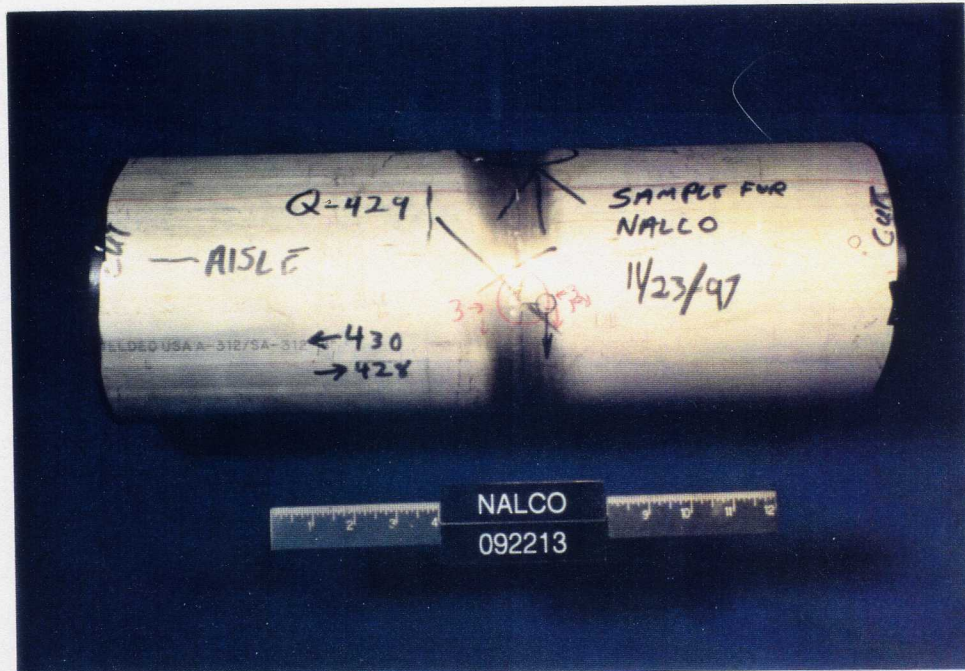


Figure 1  
As-Received Piping Section with Weld Q-429

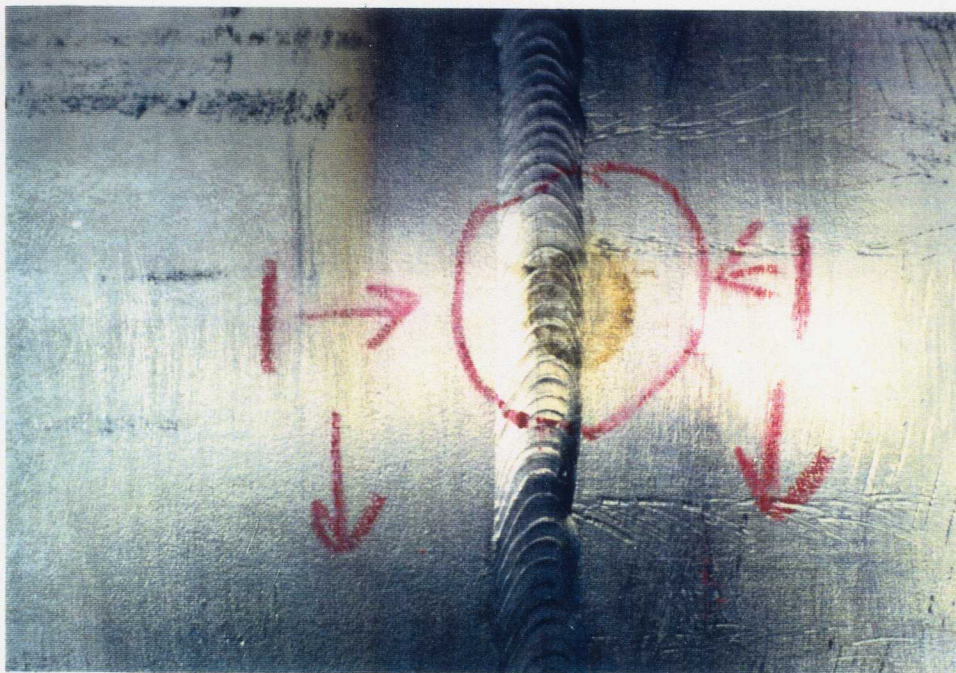


Figure 2  
Region One Showing a Brown Deposit  
On the External Surface of the Weld

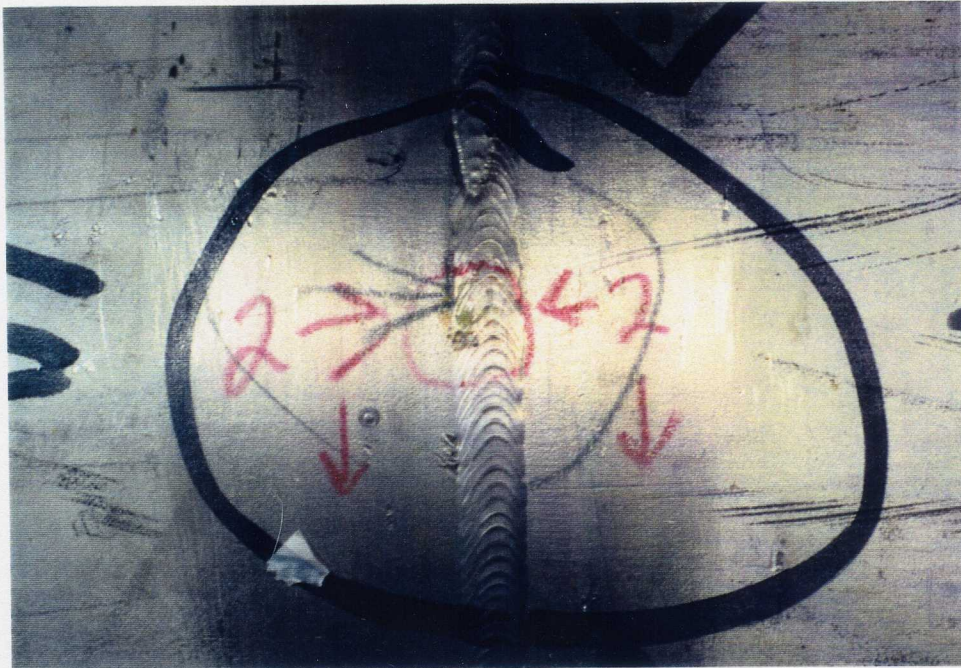


Figure 3  
Region Two Showing Small Deposit Spots

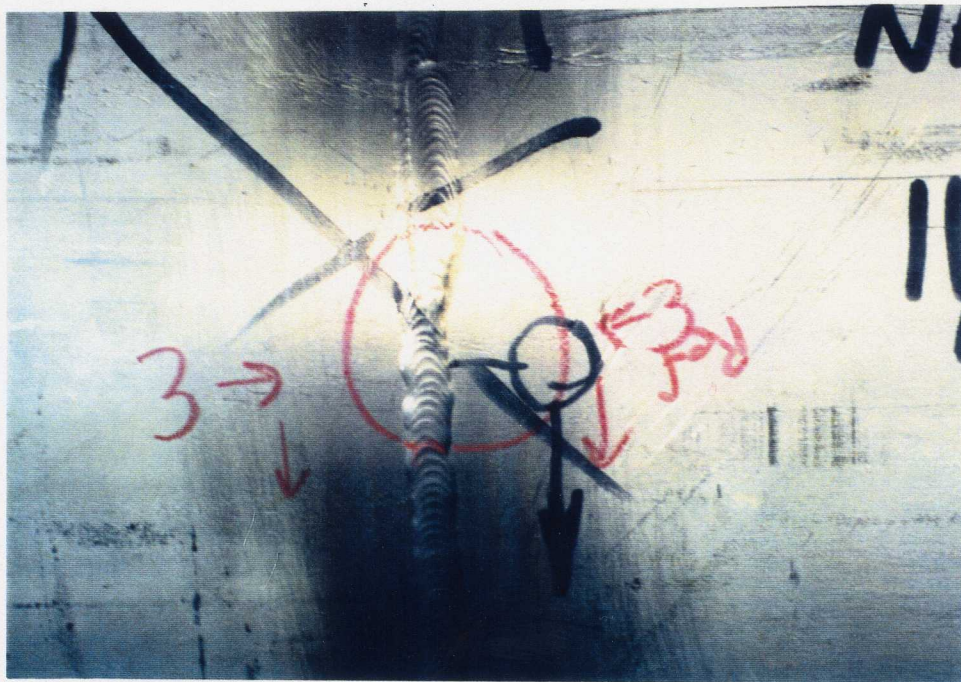


Figure 4  
Region Three Showing a Narrow Deposit Strip  
At the End of an Overlapping Weld

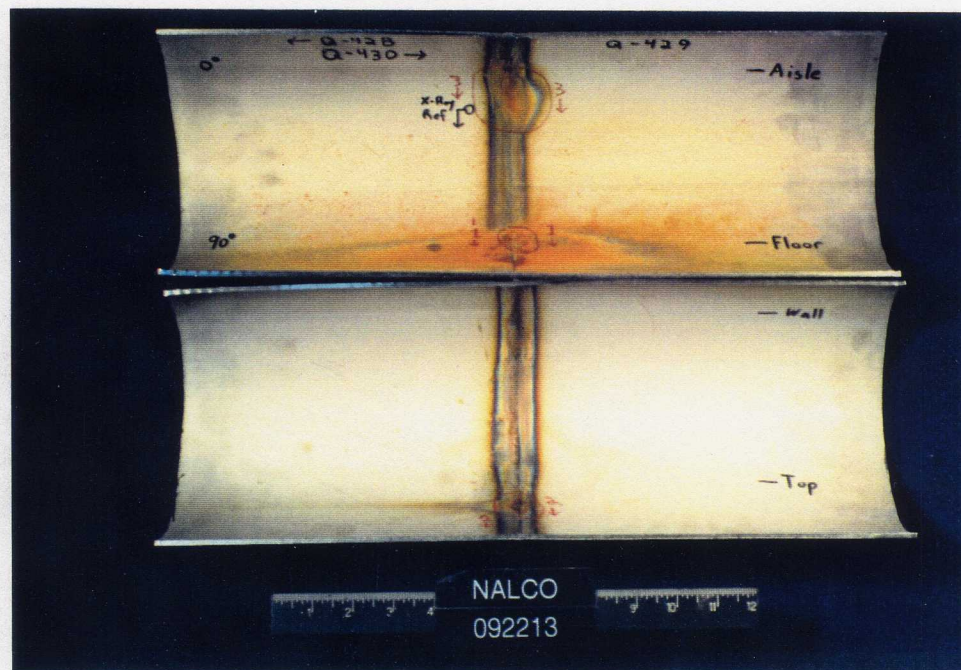


Figure 5  
Internal Surface of Piping Section Revealed  
After Longitudinal Splitting



Figure 6  
Region One Showing Misalignment of Pipes  
At the Circumferential Weld



Figure 7  
Region One Showing Corrosion Products



Figure 8  
Region Two Showing a Corrosion Nodule



Figure 9  
Close-up of Corrosion Nodule in Region Two  
Magnification: 6X



Figure 10  
Close-up of Corrosion Nodule in Region Two After Cleaning  
Magnification: 6X

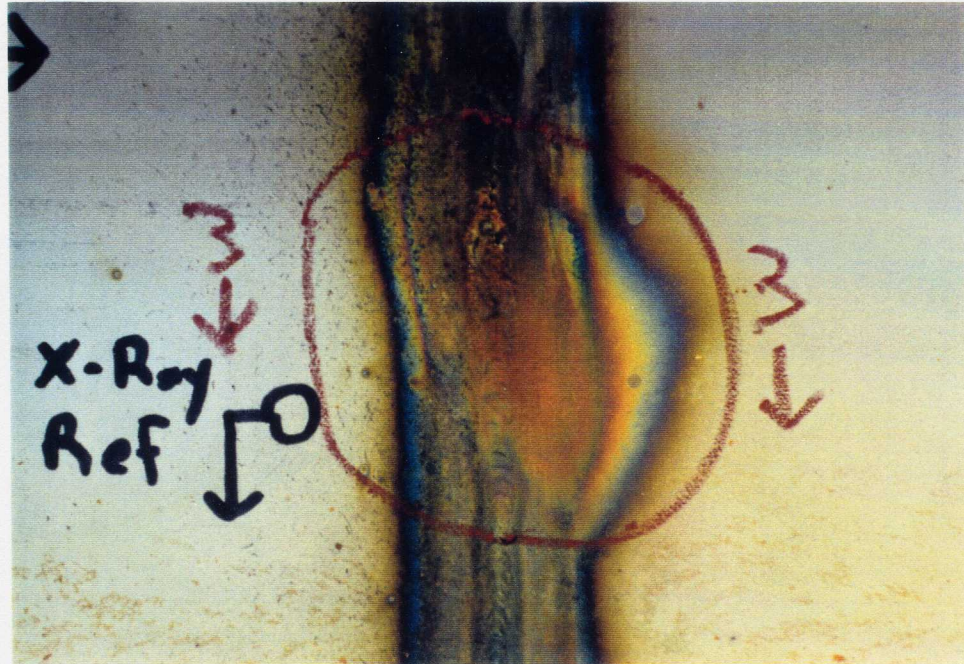


Figure 11  
Region Three Showing Corrosion at Weld

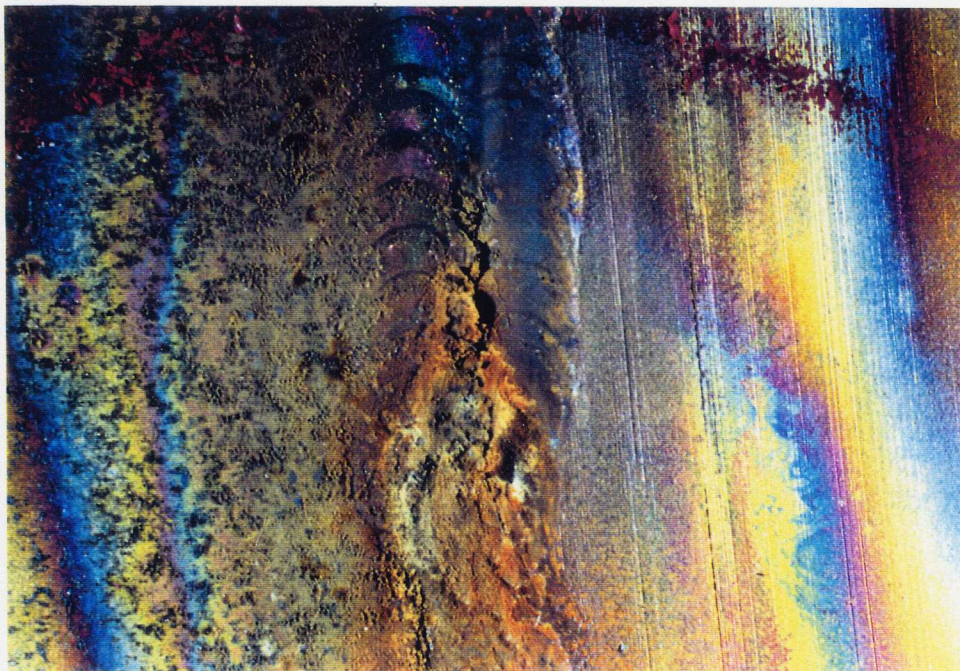


Figure 12  
Close-up of Region Three Showing Crevice Present Between Welds

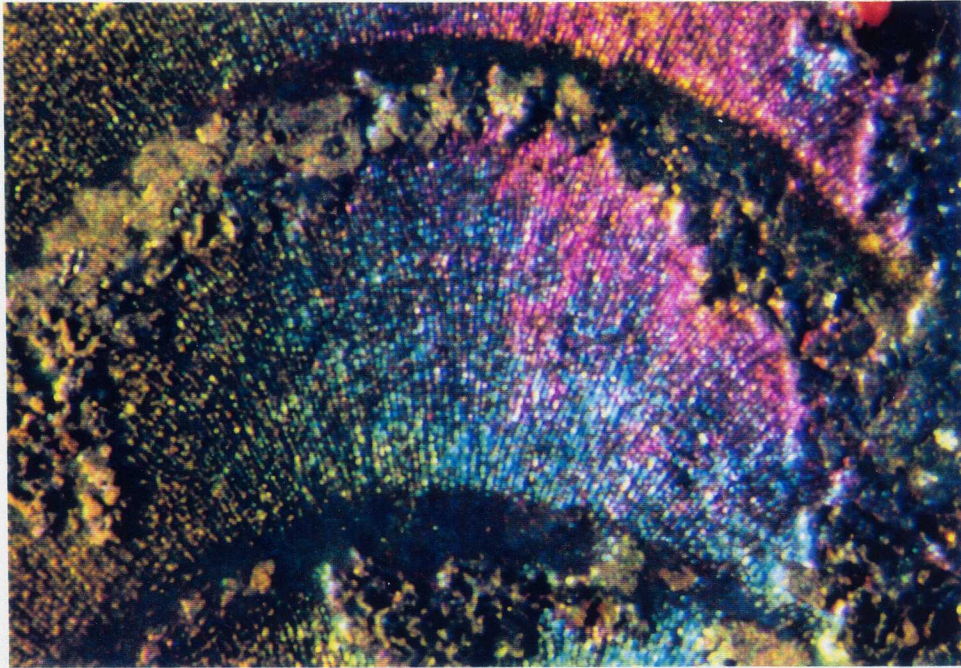


Figure 13  
Close-up in Region Three Showing Dendritic Structure of Weld  
Magnification: 25X

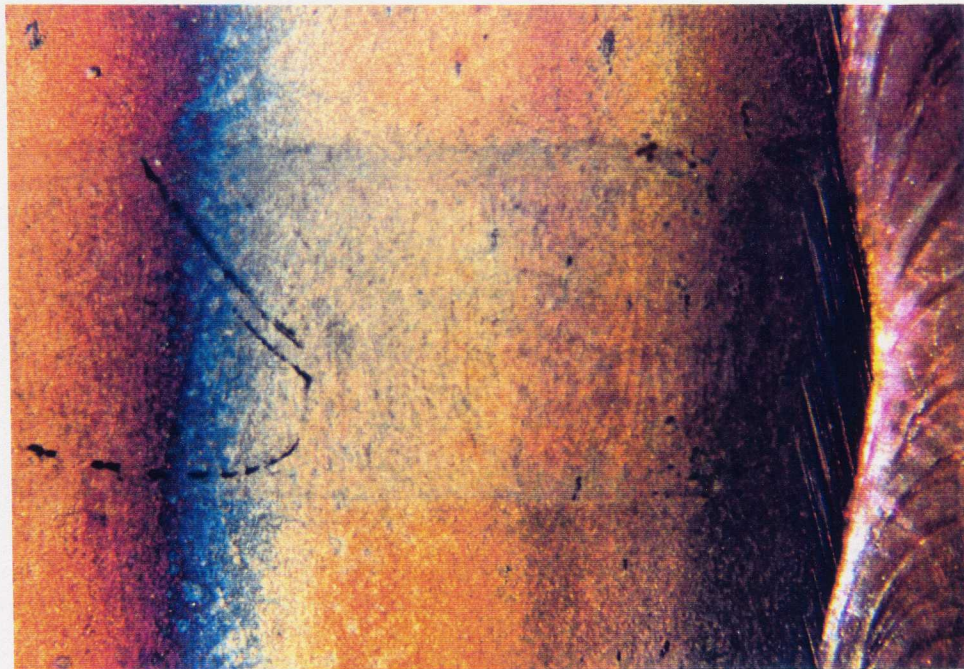


Figure 14  
Coarse Grinding Marks Along Circumferential Weld  
And Longitudinal Weld Seam

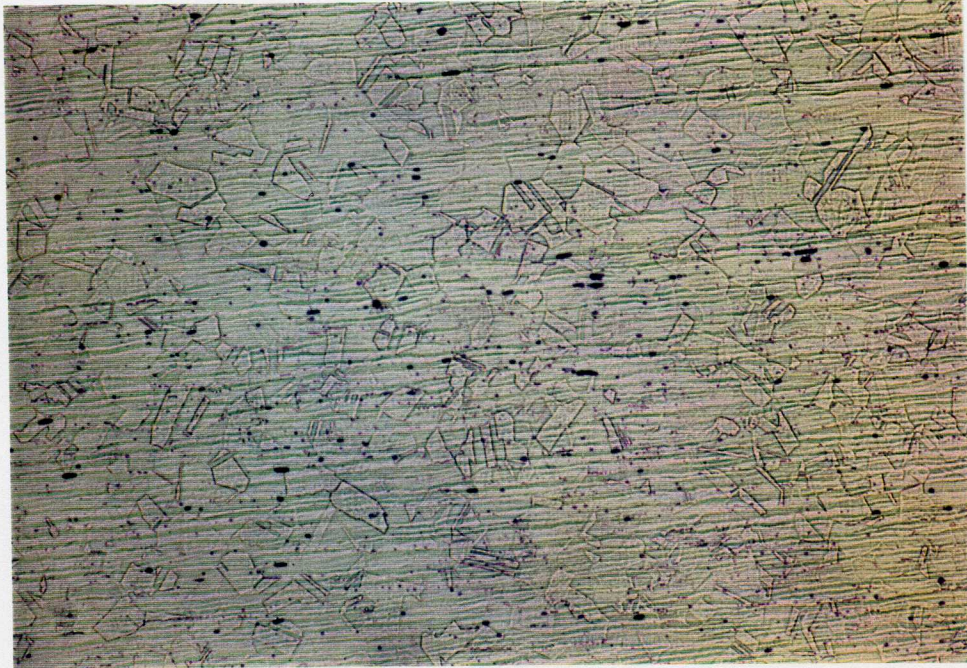


Figure 15  
Microstructure in a Transverse Section Through the Pipe  
Magnification: 200X Etchant: Electrolytic Oxalic

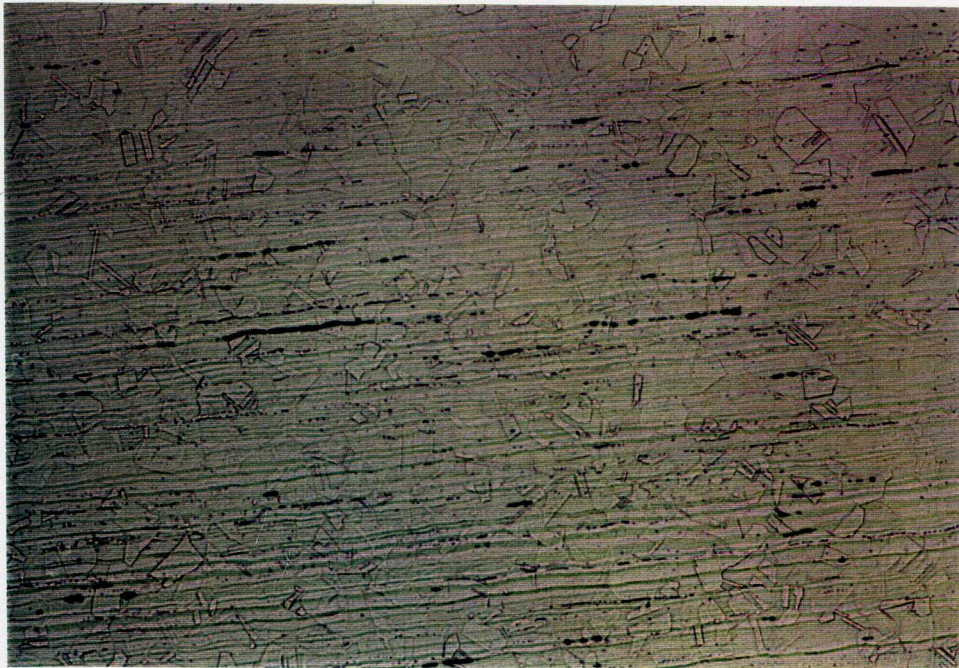


Figure 16  
Microstructure in a Longitudinal Section Through the Pipe  
Magnification: 200X Etchant: Electrolytic Oxalic

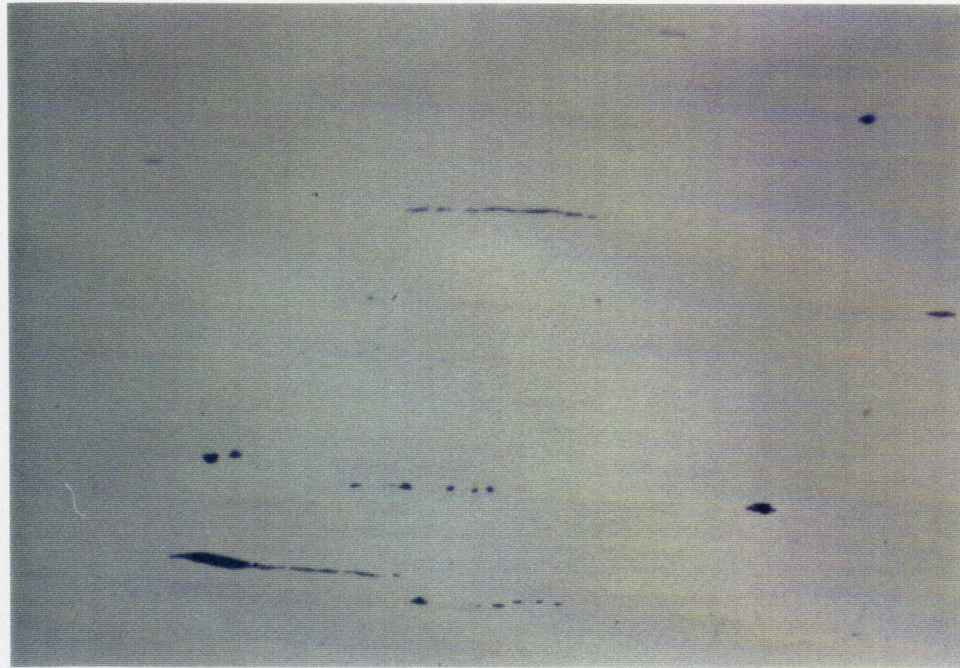


Figure 17  
Microstructure in a Longitudinal Section  
Through the Pipe Showing Inclusions  
Magnification: 500X Etchant: None



Figure 18  
Microstructure of the Longitudinal Seam Weld in Pipe  
Magnification: 25X Etchant: Electrolytic Oxalic

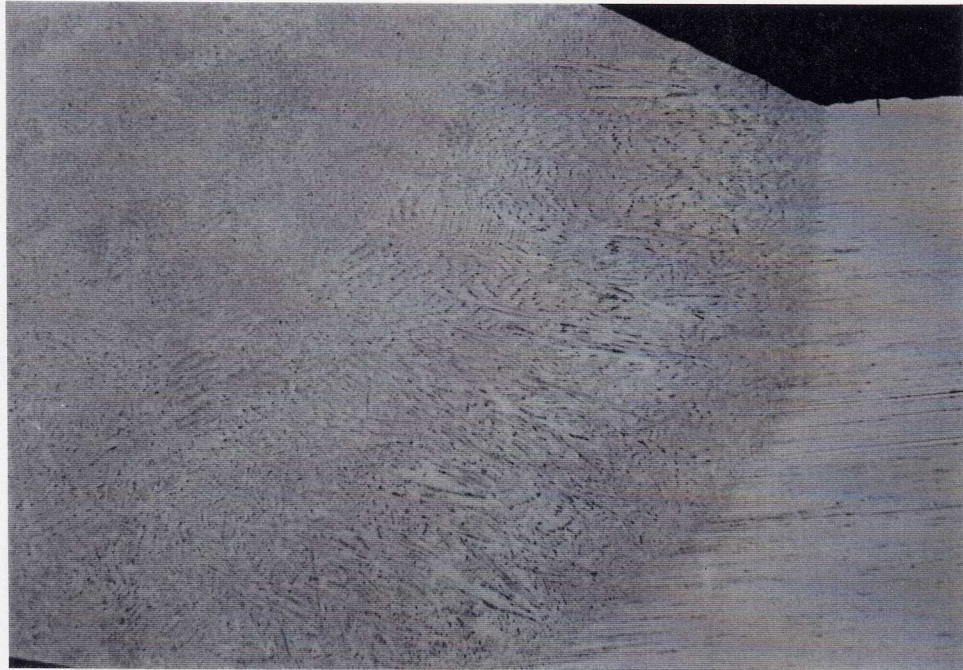


Figure 19  
Microstructure of the Circumferential Weld Joining the Pipes  
Magnification: 25X Etchant: Electrolytic Oxalic



Figure 20  
Close-up of the Microstructure of the Circumferential Weld  
Magnification: 100X Etchant: Electrolytic Oxalic



Figure 21  
External Surface of a Pipe Located Away  
From the Circumferential Weld  
Magnification: 500X Etchant: None



Figure 22  
Internal Surface of a Pipe Located Away  
From the Circumferential Weld  
Magnification: 500X Etchant: None

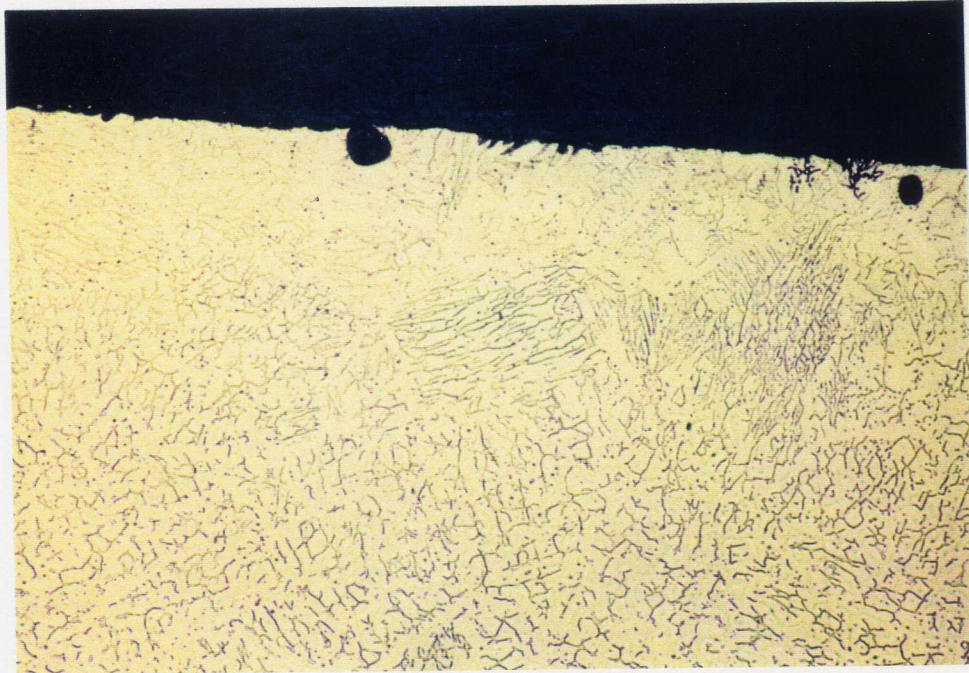


Figure 23  
External Surface of the Circumferential Weld in Region One  
Magnification: 200X Etchant: Electrolytic Oxalic



Figure 24  
Close-up of Dendritic Attack Along the External Surface  
Magnification: 1000X Etchant: Electrolytic Oxalic  
Differential Interference Contrast

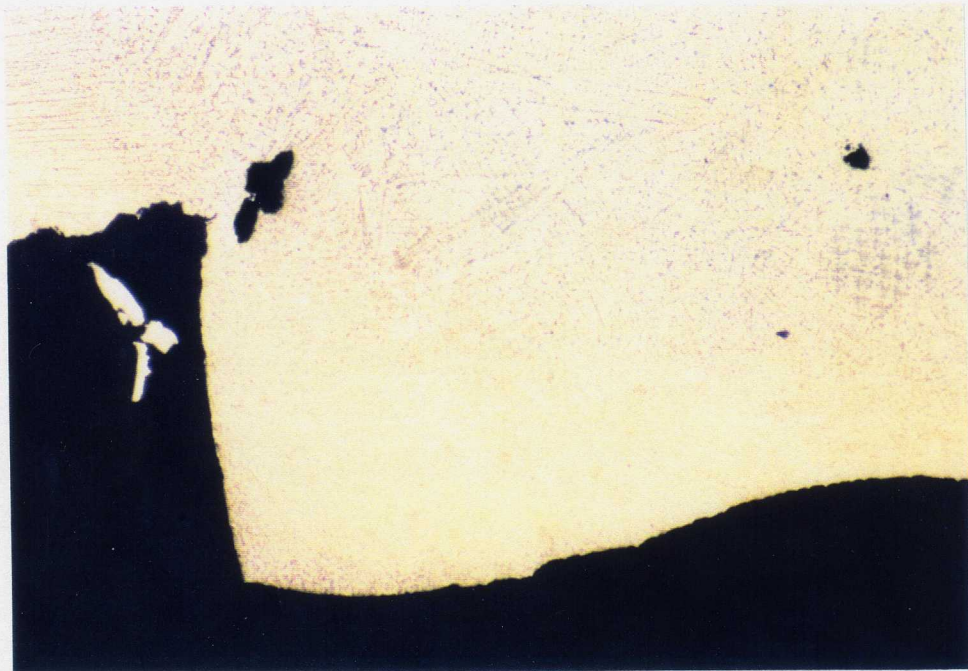


Figure 25  
Internal Surface of Circumferential Weld Showing Misalignment,  
Incomplete Fusion, and Small Cavities in Region One  
Magnification: 25X      Etchant: Electrolytic Oxalic



Figure 26  
Pit Located in Region One  
Magnification: 25X      Etchant: Unetched



Figure 27  
Edge of Pit in Figure 26 Showing Preferential Attack  
Of the Dendritic Phase  
Magnification: 200X Etchant: Unetched

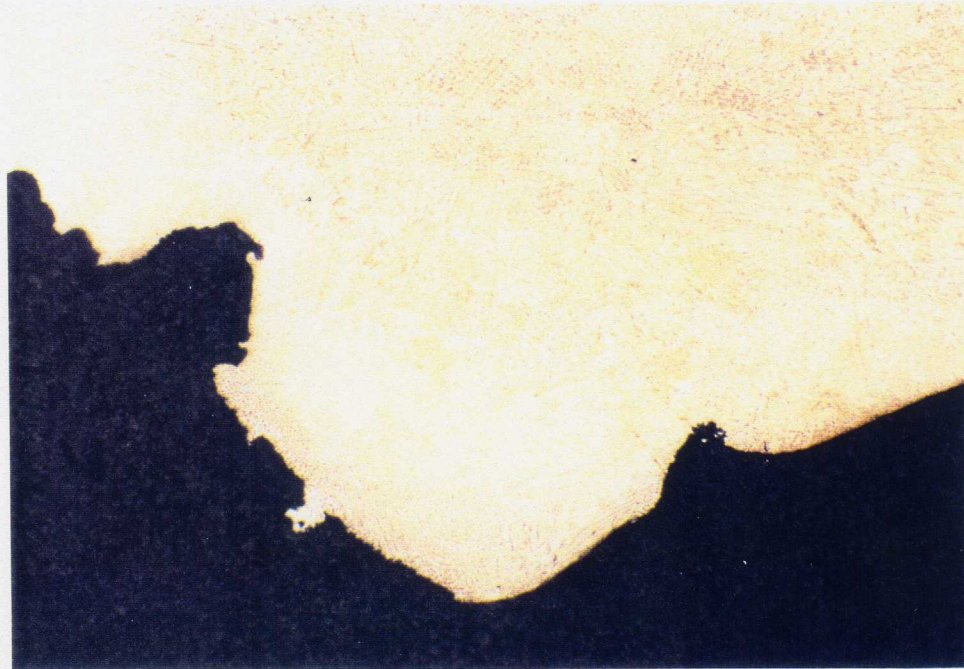


Figure 28  
Cross-Section of the Nodule Located on the  
Internal Surface in Region Two  
Magnification: 25X Etchant: Electrolytic Oxalic

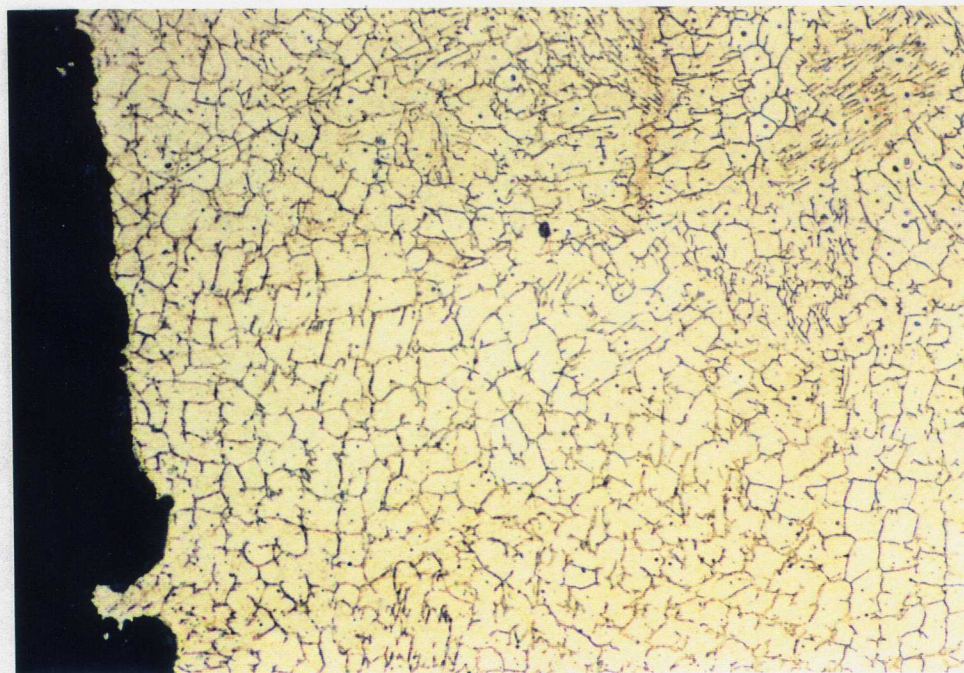


Figure 29  
Microstructure Present Along the Edge of the Nodule  
Showing an Interconnected Dendritic Phase  
Magnification: 200X Etchant: Electrolytic Oxalic

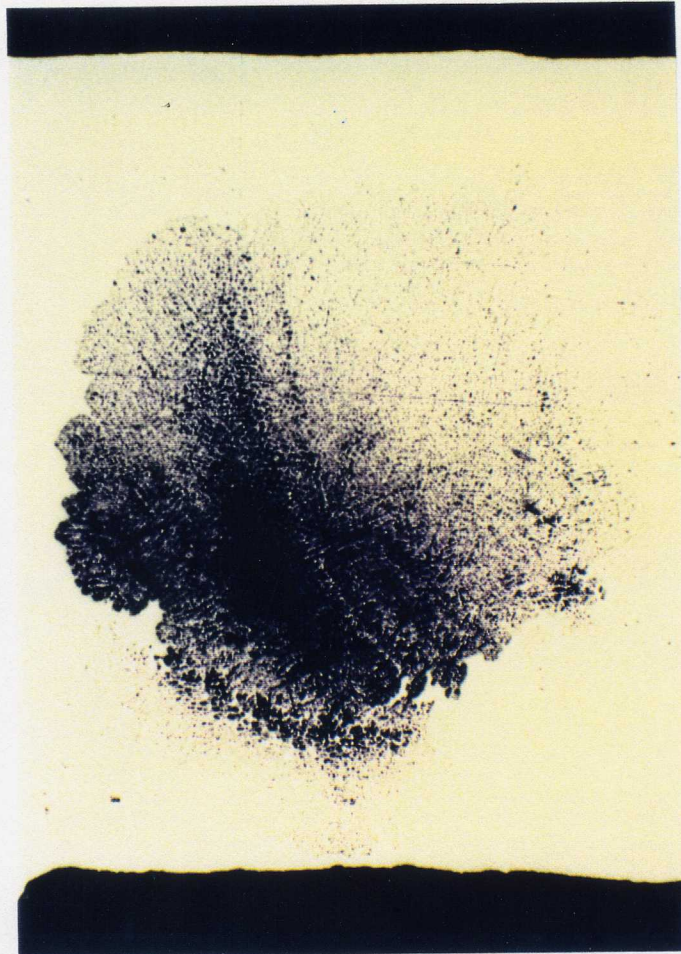


Figure 30  
Pit Located in Region Two  
Magnification: 25X      Etchant: Unetched



Figure 31  
Microstructure in the Pit Region Showing Preferential  
Attack of the Dendritic Phase  
Magnification: 200X      Etchant: Unetched

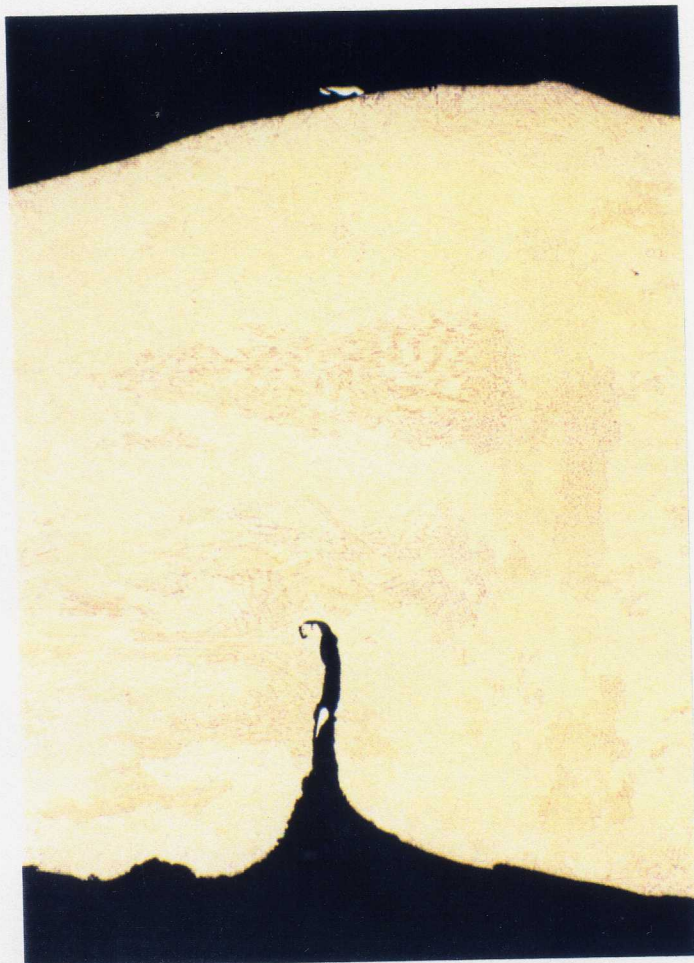


Figure 32  
Crevice Present Along the Internal Surface in Region Three  
Magnification: 25X      Etchant: Electrolytic Oxalic

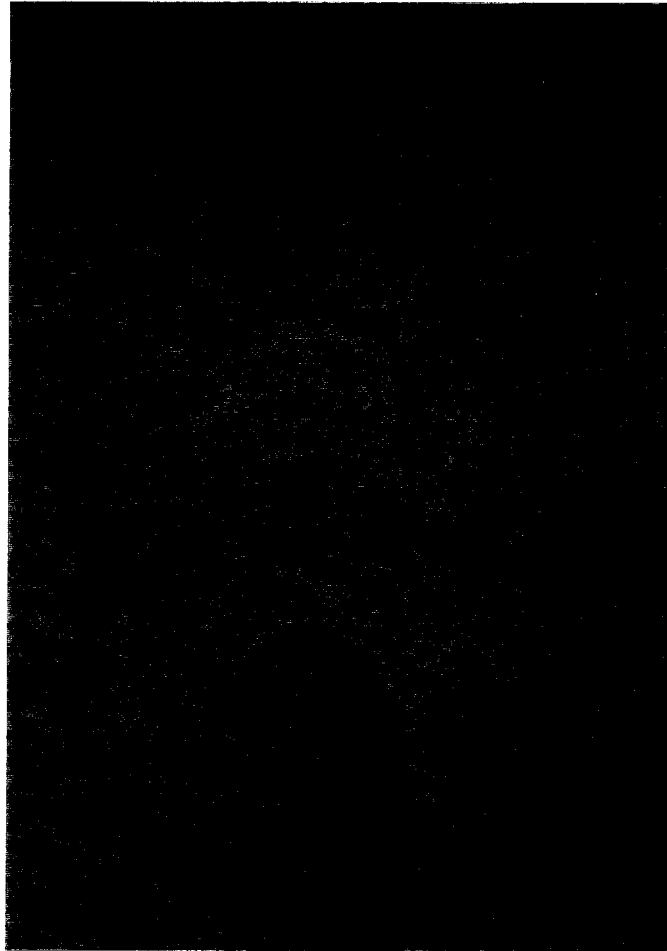


Figure 33  
Close-up of the Tip of the Crevice in Figure 32  
Magnification: 100X      Etchant: Electrolytic Oxalic



Figure 34  
Crevice Present Along the Internal Surface  
Magnification: 50X Etchant: Unetched

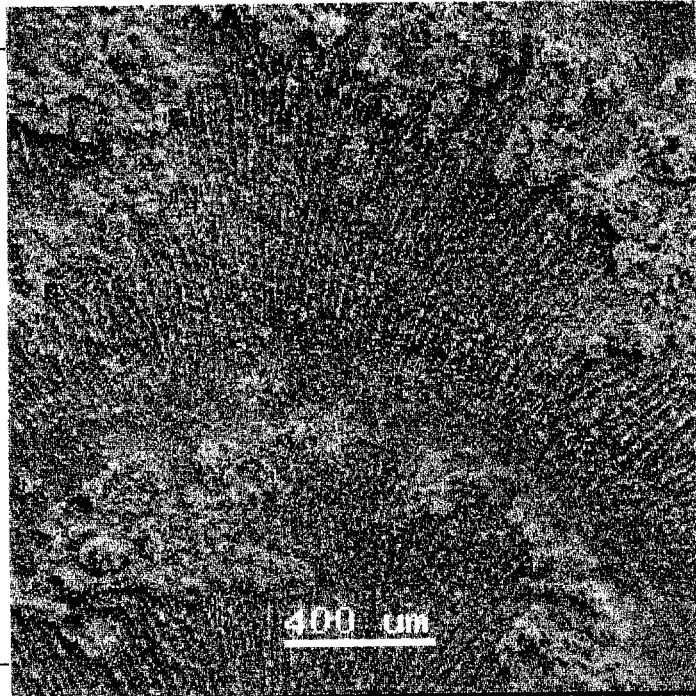


Figure 35  
SEM Photo of Surface Lying Dendritic Structure  
On Internal Surface of Weld Bead  
Magnification: 50X

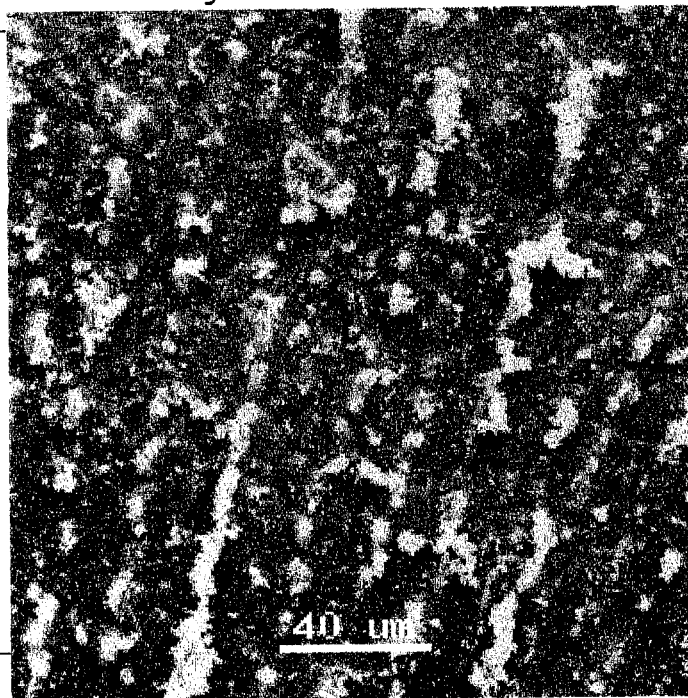


Figure 36  
Higher Magnification of Figure 35  
Magnification: 500X

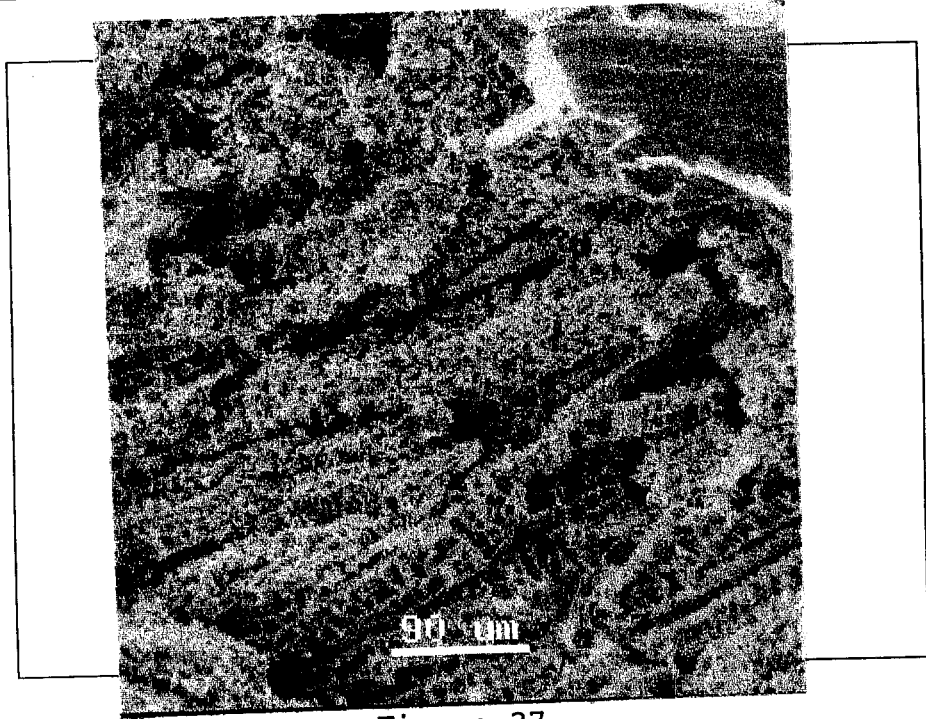


Figure 37  
SEM Photo of Interdendritic Remnants Present  
Inside Pit Located in Region One  
Magnification: 200X

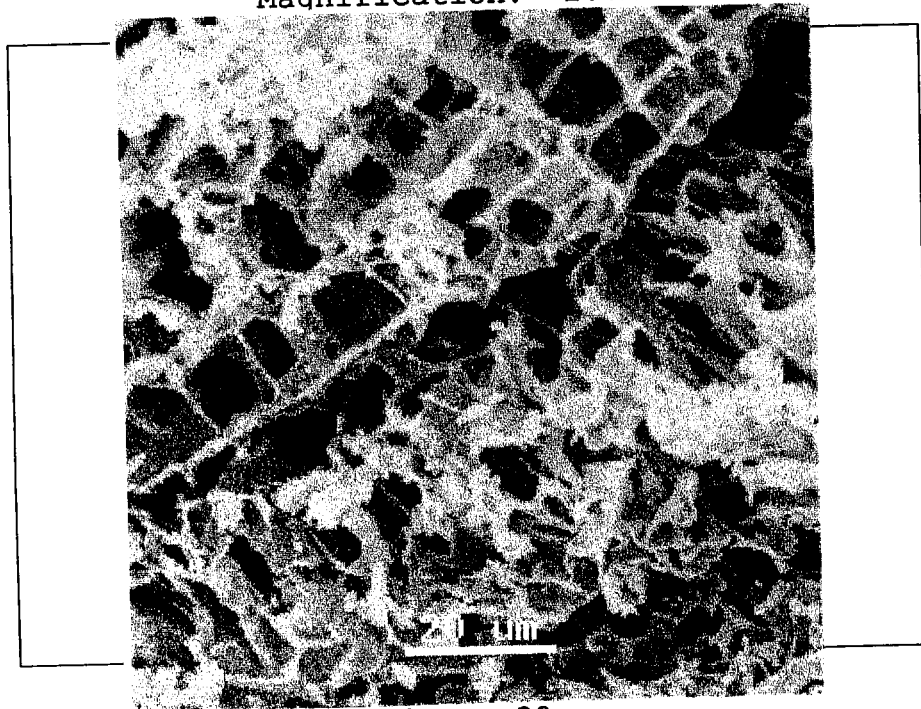
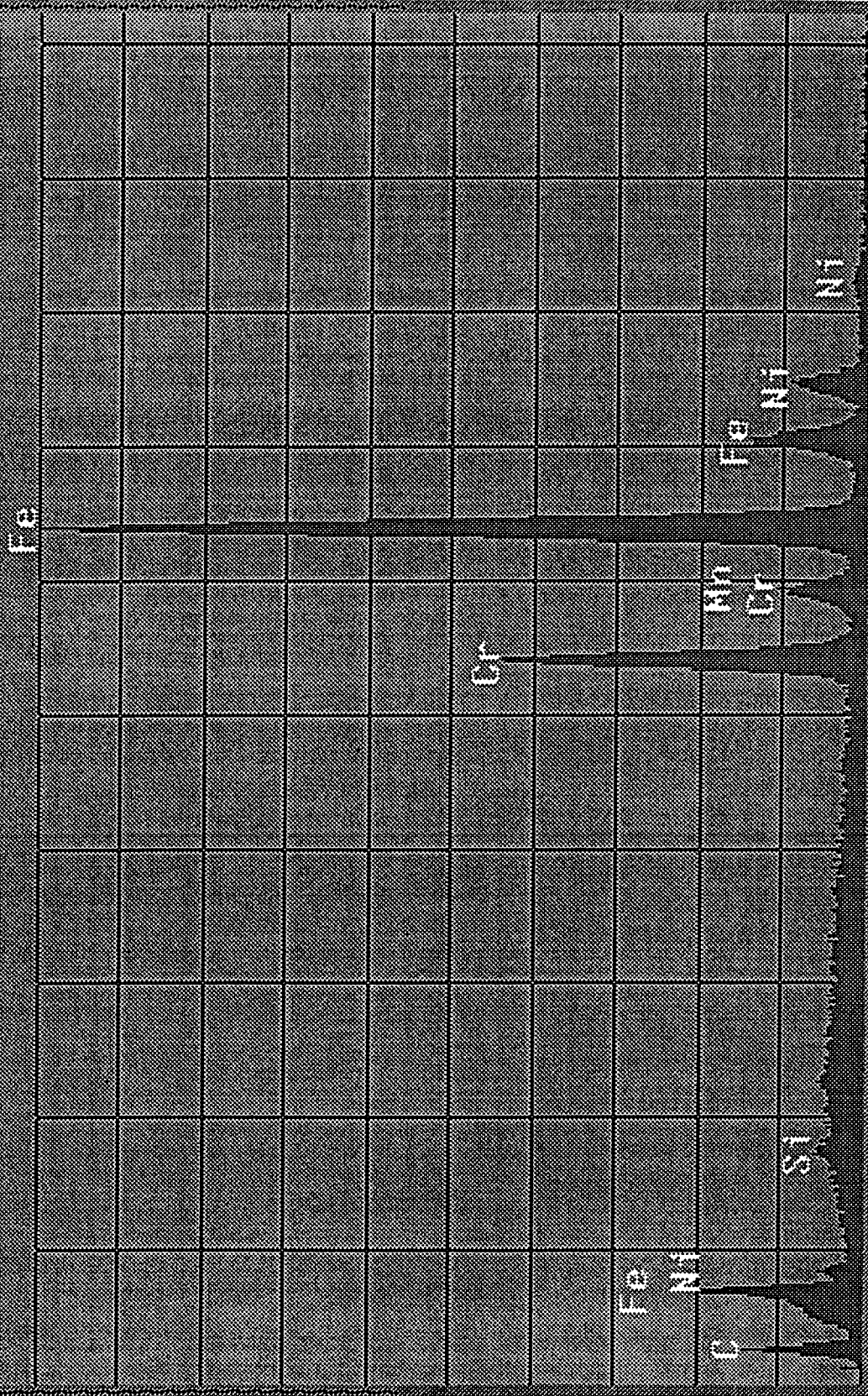


Figure 38  
Higher Magnification of Figure 37  
Magnification: 1000X

NALCO Display - Spectrum 2

VFS: 2000

Livetime: 51



0.000

keV

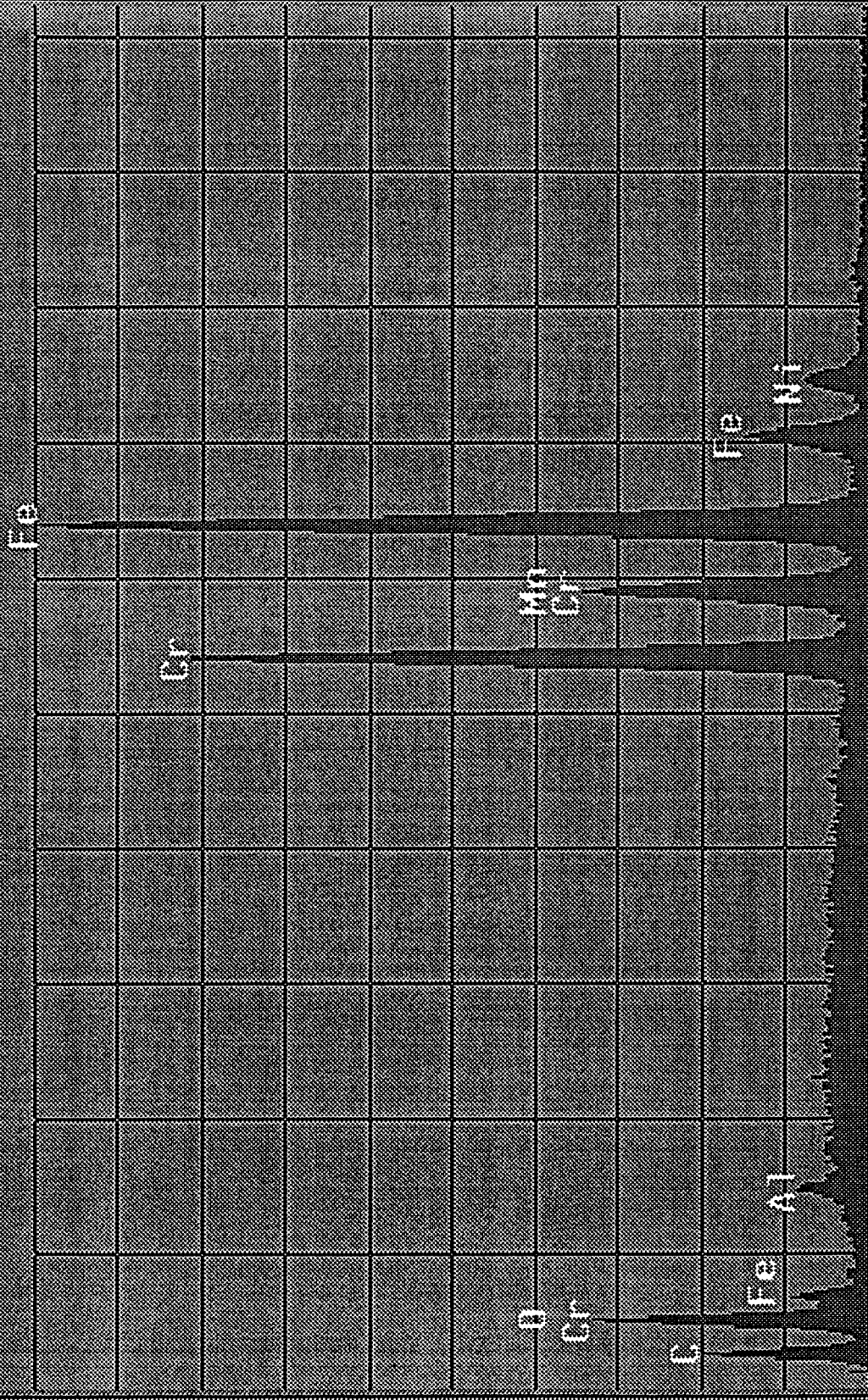
10.220

Label: 499243x alloy @ center of weld

# NALCO Display - Spectrum 3

VFS: 2000

Livetime: 70



0.000

keV

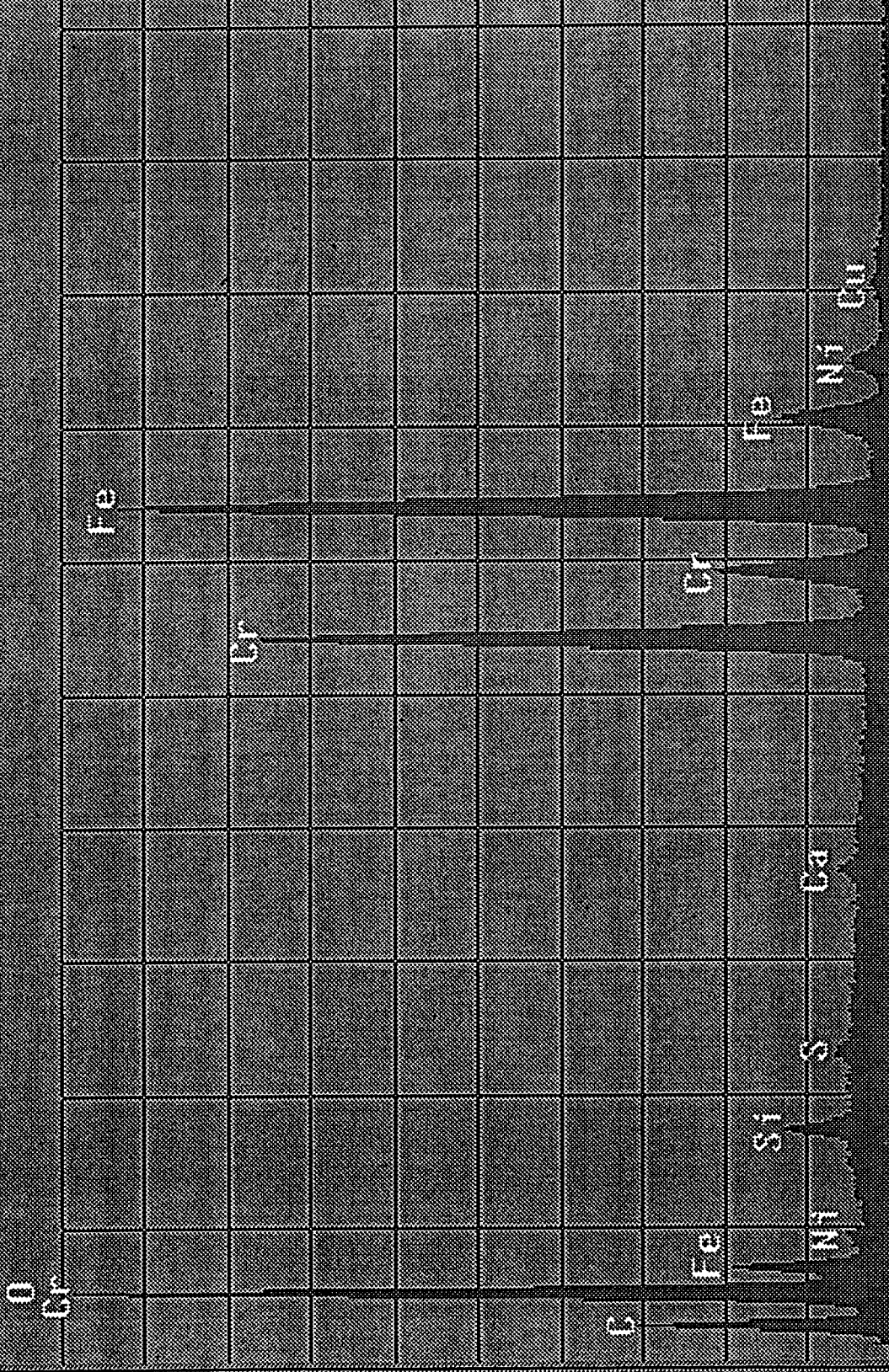
10.220

Label: 499243b inclusion site

NAEDU Display - Spectrum 2

VFS: 2000

Livetime: 73



0.000

keV

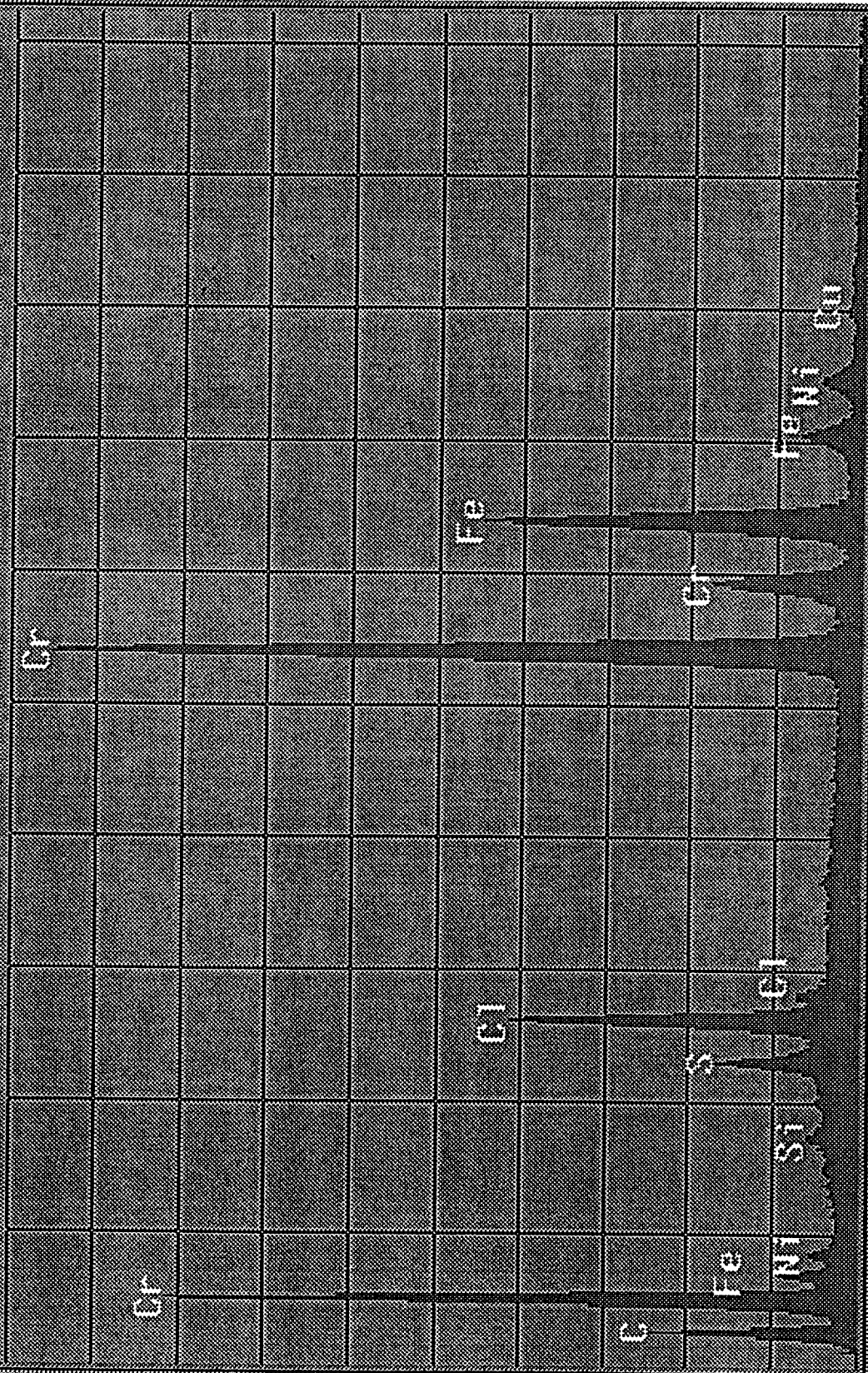
10.220

Label: 498989x sample B, residue at weld seam

**HALCO Display - Spectrum 1**

VFS: 2000

Livetime: 87



**0.000**

**key**

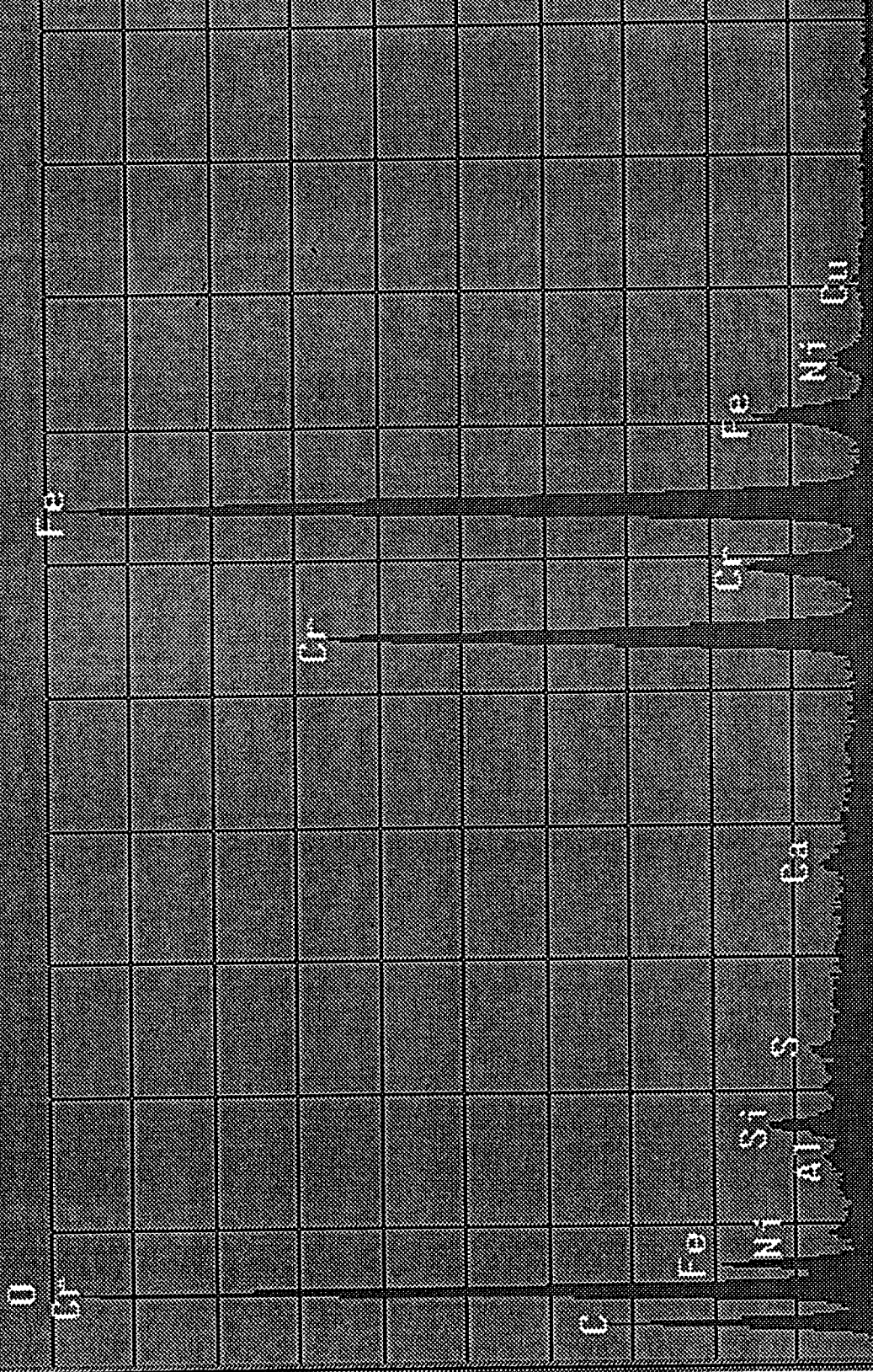
**10.220**

**Label: 498989y sample A, deposit/corr. residue**

# HALO Display - Spectrum 7

VFS: 2000

Livetime: 58



0.000

keV

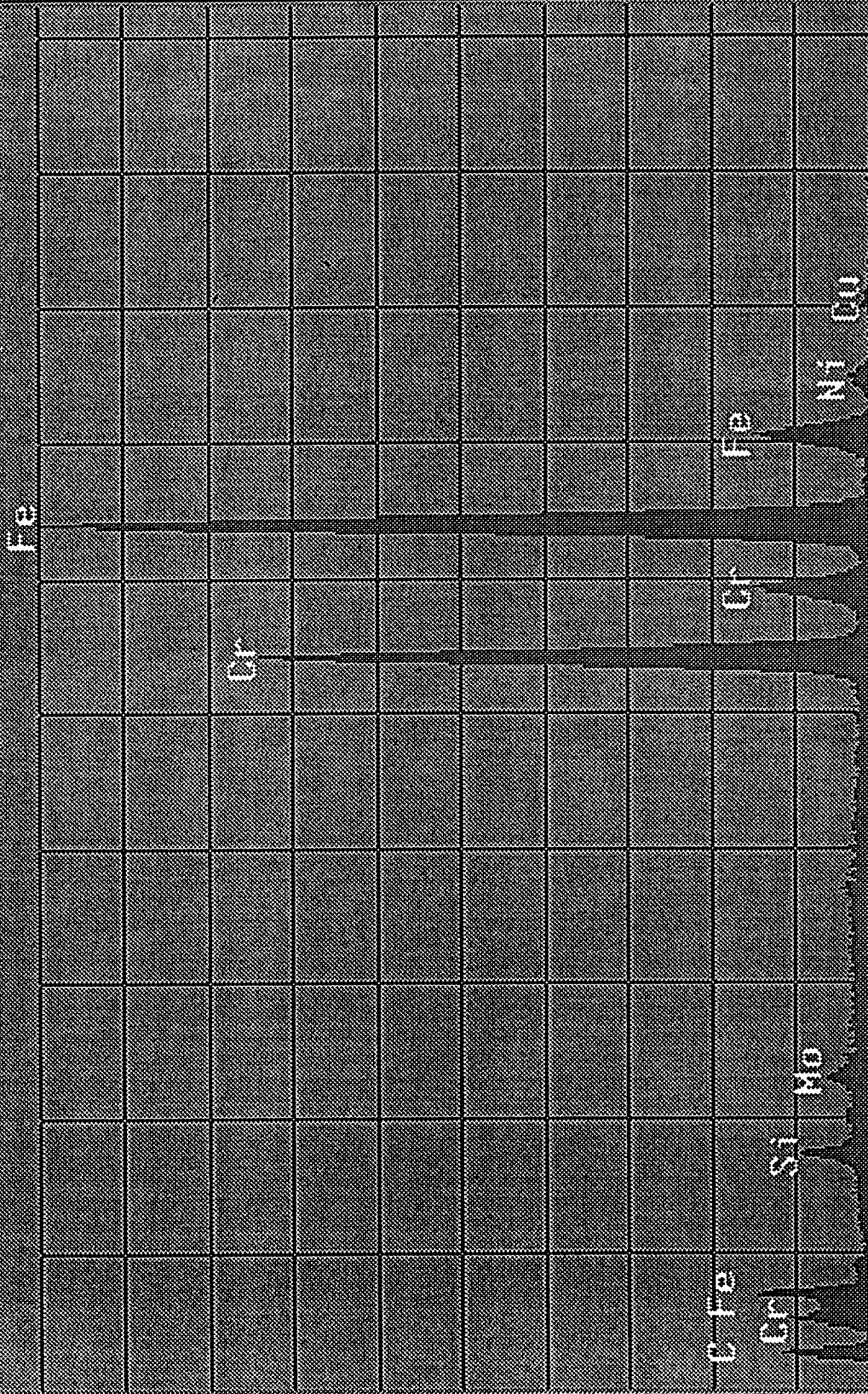
10.220

Label: 498989q sample C, bump area site

NALCO Display - Spectrum

VFS: 2000

Livetime: 43



0.000

key

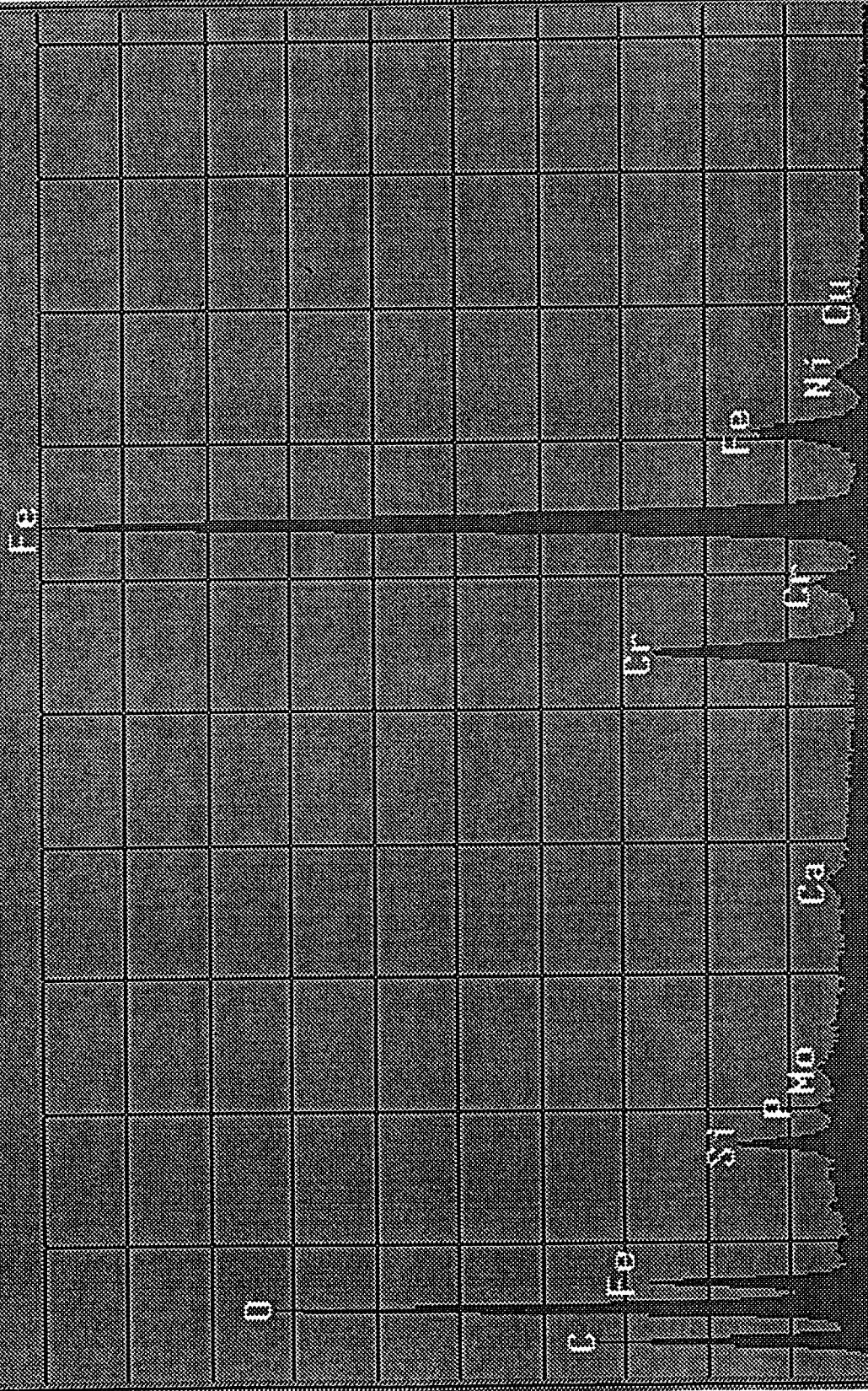
10.220

Label: 498989s sample E, dendrite rows

NALCO Display - Spectrum

VFS: 2000

Livetime: 40



0.000

keV

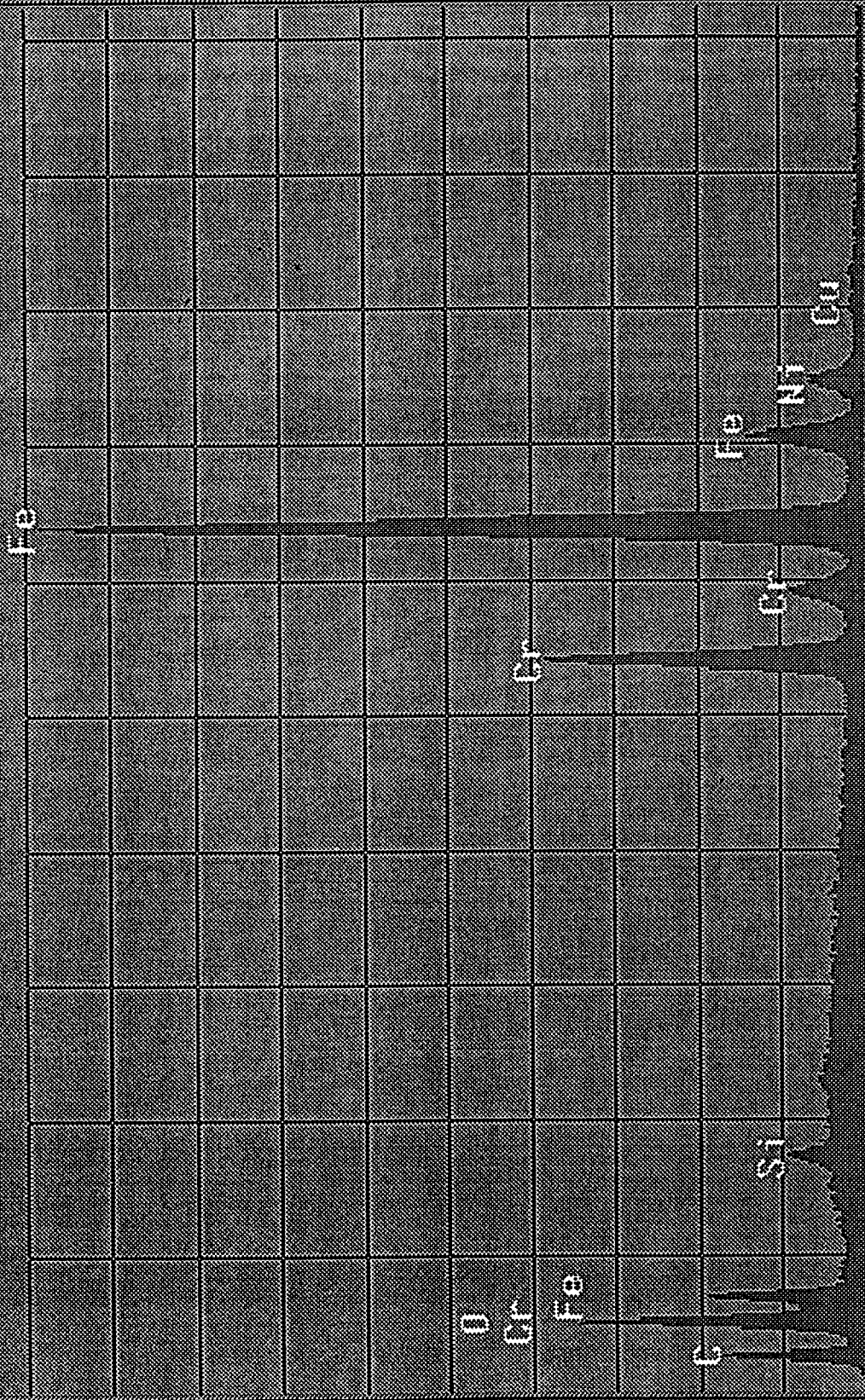
10.220

Label: 498989v sample B, fan area, coarse

NALCO Display - Spectrum 3

VFS: 2000

Livetime: 29



0.000

keV

10.220

Label: 498989w sample B, fan area, smooth